Improved Channel Estimation and Equalization for Single-Carrier IEEE 802.11ad Receivers

Giuseppe BARUFFA, Luca RUGINI

Dept. of Engineering, University of Perugia, via G. Duranti 93, 06125 Perugia, Italy

{giuseppe.baruffa, luca.rugini}@unipg.it

Submitted April 28, 2023 / Accepted July 31, 2023 / Online first August 7, 2023

Abstract. *IEEE 802.11ad uses mmWave technology for multi-gigabit wireless access networks. Multipath with large delay spread severely reduces performance due to insufficient guard interval. In this paper, we improve single-carrier IEEE 802.11ad receivers by proposing channel estimation and equalization methods for a frequency domain equalizer. Channel estimation is improved by leveraging on sparsity of the channel impulse response, while equalization is combined with an interference cancellation algorithm. The log-likelihood ratio demapper is also improved by correct power estimation of signal, interference, and noise. Simulation results show that the proposed methods are effective on channels whose length exceeds the guard interval.*

Keywords

802.11ad, MMSE equalization, sparse channel estimation, channel shortening, interference cancellation

1. Introduction

The IEEE 802.11ad standard provides a reliable and high-data rate wireless link for personal communications in the 60 GHz (mmWave) band [1]. The standard (also known as WiGig [2]) offers a dual communication method, allowing for either single-carrier (SC) or orthogonal frequency-division multiplexing (OFDM) operation over a channel bandwidth of more than 2 GHz with multi-Gbps capabilities [1], [3]. The SC method has lower power and computational requirements than the OFDM method, so it is mandatory in all compliant devices [1]: it is conceived for scenarios with short channel impulse responses (CIR), with scarcely selective frequency responses, and for handheld devices [4]. Indeed, both modes are characterized by a cyclic-prefix (CP) enabled physical layer (PHY) frame, but the CP length for SC is half the CP length of OFDM [3]. In the IEEE 802.11ad standard [3, p. 476–477], for the SC modes, the CP is denoted as guard interval (GI).

Several vendors offer mmWave devices that allow to extend 802.11ad operation beyond the scenario of indoor, short-distance communications: for instance, several commercially available products are capable to establish mmWave links as replacement of Gigabit Ethernet wired connections [5], [6]. Many of these products are based on the chipset [7], which uses the SC mode. Due to the widespread presence of SC, an important aspect is the extension of the capabilities of an IEEE 802.11ad SC device, at least at the receiving side, in order to improve performance on outdoor channels.

1.1 Literature Review

Several studies consider the performance of IEEE 802.11ad receivers. Gao et al. [8] investigate the sparsity nature of the 60 GHz channel and propose an algorithm to jointly estimate the channel response and the signal-to-noise ratio (SNR) using a pilot sequence, which is a slight modification of that of IEEE 802.11ad. Sparsity is also considered in [9] for fast channel estimation and beam tracking, but multiple-input multiple-output channels are considered and a feedback link is necessary. The method in [10] alters the pilot sequence, so as to track time-varying CIR: however, this method applies only to the OFDM mode and does not solve the problem of insufficient CP length for the SC mode. In [11–13] an implementation study of an IEEE 802.11ad receiving chip is presented. This study adopts an autocorrelation-based channel estimation method, followed by a noise-reduction step to reduce the presence of spikes in the CIR, but does not tackle the effects of self-interference. The technique in [14] uses the correlation properties of the preamble sequence to estimate the channel and the SNR, and implements the synchronization and equalization blocks in an FPGA, showing that high throughput is possible. The paper [15] presents the performance of an IEEE 802.11ad SC MATLAB simulator that includes additional modulations and coding schemes with respect to those defined in the standard [3]. A specific feature of [15] is the use of the 60 GHz indoor channel model [16], [17], obtained from measurements done in Brno, Czech Republic. A performance study of IEEE 802.11ad is also done in [18], where the 60 GHz channel is modeled using a Rician distribution.

DOI: 10.13164/re.2023.0438

All the above methods do not consider in an explicit way the interblock interference (IBI) generated when the length of the CIR is excessive. A method to reduce the IBI is presented in [19] by exploiting the reconstruction of a longer CP in an iterative manner. Noise reduction in the reconstructed data utilize either the outputs of a soft channel decoder, or some precoding added to the transmitted signal. A similar approach to IBI cancellation is also described in [20], which proposes a frequency domain equalizer that considers the presence of residual IBI in the signal.

A third set of IEEE 802.11ad papers focuses on radar purposes. The method of [21] uses IEEE 802.11ad waveforms as joint radar/communication signal in an automotive scenario, showing that a range precision of 0.1 m is possible by exploiting the properties of the frame preamble. Also in [22] IEEE 802.11ad is used for opportunistic radar purposes: the method in [22] removes the interference from previous reflections so as to provide a multiple-target detection capability. In [23], a novel set of optimized sequences is proposed for joint multi-user communication and radar sensing, while in [24] a study is performed concerning the mutual interference between communication and radar. Other recent studies about IEEE 802.11ad include modulation classification [25], velocity estimation by autocorrelation methods [26], and comparison with other standards for vehicle-to-everything (V2X) applications [27], [28].

1.2 Contribution

In this paper we present a method to improve channel estimation at the receiver using the actual preamble syntax of IEEE 802.11ad. The newly proposed channel estimators are based on reduced-size inversion and minimum mean-squared error (MMSE), and are designed in such a way to exploit the CIR sparsity and the CIR covariance. This prior knowledge about the CIR is acquired by a preliminary coarse estimation of the CIR itself using an existing cross-correlation method [11]. Simulation results show that the proposed channel estimators outperform the existing channel estimators based on cross-correlation [11] and on full-size inversion [8].

In parallel, we propose to improve the detection for SC IEEE 802.11ad systems, by exploiting MMSE equalization with interference cancellation, so as to counteract multipath channels whose duration exceeds the GI. Specifically, we propose a new IBI-cancellation-based MMSE equalizer that incorporates the proposed channel estimator. In addition to IBI cancellation, the proposed equalizer also restores the circularity property that is lost after cancellation. This restoration makes the frequency-domain channel matrix diagonal and enables low-complexity equalization. Simulation results show that the proposed MMSE equalization with IBI canceler outperforms frequency-domain equalizers without IBI cancellation [11], [12], and CIR shortening methods existing in the literature [29–32].

In addition, we also propose a log-likelihood ratio (LLR) update algorithm tailored to the proposed equalizer, based on the estimation of the amount of residual interference after IBI cancellation. Simulation results show that the proposed LLR update with residual interference estimation outperforms the conventional LLR calculation [33].

1.3 Paper Organization and Notation

The remainder of this paper is organized as follows. Section 2 details the mathematical model of the IEEE 802.11ad SC standard. Section 3 presents the existing and the proposed channel estimation schemes. Detection is the subject of Sec. 4, which also includes equalization, IBI cancellation, channel shortening, and LLR update. Section 5 shows the results of the simulations and compares the performance of the proposed methods with the existing ones. Finally, Section 6 concludes the paper.

This paper uses the following notation. Lowercase letters represent vectors and uppercase letters represent matrices, $\mathbf{I}_n$ is the identity matrix of size n, $\mathbf{0}_{n\times m}$ and $\mathbf{1}_{n\times m}$ are the all-zero and all-ones $n \times m$ matrices, $\otimes$ represents the Kronecker product operator, $\odot$ is the Hadamard product operator, b_n represents the nth entry of vector $\mathbf{b}$, $B_{m,n}$ represents the element at row m and column n of $\mathbf{B}$, and $\mathbf{b}_i$ is the ith column vector of $\mathbf{B}$. We define $\mathrm{Toep}(\mathbf{a};\mathbf{b}^{\mathrm{T}})$ as the Toeplitz matrix with $\mathbf{a}$ as first column and $\mathbf{b}^{\mathrm{T}}$ as first row, $\mathrm{Unvec}_{m,n}(\mathbf{b})$ as the $m\times n$ matrix that contains the elements of $\mathbf{b}$ columnwise, $\mathrm{vec}(\mathbf{B})$ as the vectorization operator that stacks the columns of a matrix into a single vector, $\mathrm{Diag}(\mathbf{b})$ as the diagonal matrix of $\mathbf{b}$, $\mathrm{diag}(\mathbf{B})$ as the column vector that contains the diagonal of $\mathbf{B}$, $\mathrm{tr}(\mathbf{B})$ as the trace of $\mathbf{B}$, and $(\cdot)_n$ as the element-wise modulo-n operation. The 0-norm $\|\mathbf{a}\|_0$ defines the sparsity of $\mathbf{a}$, i.e., the number of non-zero entries. Moreover, δ_n is the Kronecker delta. A complex random variable x with mean value η_x and variance $\sigma_x^2/2$ on both real and imaginary parts is denoted with $x \sim \mathcal{CN}(\eta_x, \sigma_x^2)$, while $i \sim \mathcal{U}\{a, b\}$ is an integer random variable uniformly distributed between a and b. $\mathrm{E}\{\cdot\}$ is the statistical expectation operator.

2. IEEE 802.11ad System Model

IEEE 802.11ad uses control and data frames. Both types of frames are introduced by a preamble, composed of a short training field (STF) used for synchronization [11], [13], and of a channel estimation field (CEF). The preamble of data frames is followed by a header, which conveys signaling information. A data part concludes the frame.

2.1 Preamble Part

For channel estimation purposes, we derive a mathematical model that expresses the received signal as a function of the STF and CEF. These fields are obtained by repeating and concatenating two complementary Golay sequences (GS) [34], as expressed by

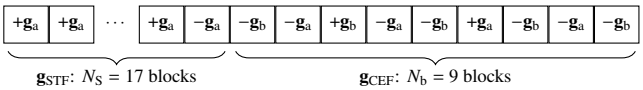

Fig. 1. Preamble for IEEE 802.11ad SC data frames.

$$\mathbf{g}_{\mathrm{STF}} = (\mathbf{S}_{\mathrm{STF}} \otimes \mathbf{I}_{L_\mathrm{b}})\mathbf{g}_\mathrm{a}, \tag{1a}$$

$$\mathbf{g}_{\mathrm{CEF}} = (\mathbf{S}_{\mathrm{CEF}} \otimes \mathbf{I}_{L_\mathrm{b}}) \begin{bmatrix} \mathbf{g}_\mathrm{a} \\ \mathbf{g}_\mathrm{b} \end{bmatrix} \tag{1b}$$

where $\mathbf{g}_{\mathrm{STF}}$ is the STF of size $N_\mathrm{S}L_\mathrm{b} \times 1$, with $N_\mathrm{S} = 17$ and block length $L_\mathrm{b} = 128$, $\mathbf{g}_{\mathrm{CEF}}$ is the CEF of size $N_\mathrm{b}L_\mathrm{b} \times 1$, with $N_\mathrm{b} = 9$, $\mathbf{g}_\mathrm{a}$ and $\mathbf{g}_\mathrm{b}$ are the two complementary GS of size L_b, $\mathbf{S}_{\mathrm{STF}} = [\, \mathbf{1}_{1\times(N_\mathrm{S}-1)} \;\; -1 \,]^\mathrm{T}$, and

$$\mathbf{S}_{\mathrm{CEF}} = \begin{bmatrix} 0 & -1 & 0 & -1 & 0 & +1 & 0 & -1 & 0 \\ -1 & 0 & +1 & 0 & -1 & 0 & -1 & 0 & -1 \end{bmatrix}^\mathrm{T}. \tag{2}$$

The structure of the preamble[1] is shown in Fig. 1 for SC transmission mode. This preamble is transmitted after phase rotation, as expressed by

$$\mathbf{c} = \begin{bmatrix} \mathbf{c}_{\mathrm{STF}} \\ \mathbf{c}_{\mathrm{CEF}} \end{bmatrix}, \tag{3a}$$

$$\mathbf{c}_{\mathrm{STF}} = \mathbf{R}_{N_\mathrm{S}L_\mathrm{b}}\mathbf{g}_{\mathrm{STF}}, \tag{3b}$$

$$\mathbf{c}_{\mathrm{CEF}} = \mathbf{R}_{N_\mathrm{b}L_\mathrm{b}}\mathbf{g}_{\mathrm{CEF}} \tag{3c}$$

where $\mathbf{R}_N = \mathrm{Diag}([\, 1 \;\; \exp(\mathrm{j}\frac{\pi}{2}) \;\; \ldots \;\; \exp(\mathrm{j}(N-1)\frac{\pi}{2}) \,])$ represents a $\pi/2$ rotation matrix of N samples used for peak-to-average power ratio reduction [1]. After convolution with the time-invariant CIR $\mathbf{h}$ of length L_h, which includes the effects of transmit and receive filters, the received signal $\mathbf{p}$ (with $N_\mathrm{b}L_\mathrm{b}$ samples corresponding to the CEF part) is expressed by[2]

$$\mathbf{p} = \mathbf{C}\mathbf{h} + \mathbf{w}, \tag{4}$$

$$\mathbf{C} = \mathrm{Toep}(\mathbf{c}_{\mathrm{CEF}}; \tilde{\mathbf{c}}), \tag{5}$$

$$\tilde{\mathbf{c}} = [\, c_{\mathrm{CEF}_0} \;\; c_{\mathrm{STF}_{N_\mathrm{S}L_\mathrm{b}-1}} \;\; c_{\mathrm{STF}_{N_\mathrm{S}L_\mathrm{b}-2}} \;\cdots\; c_{\mathrm{STF}_{N_\mathrm{S}L_\mathrm{b}-(L_\mathrm{h}-1)}} \,]. \tag{6}$$

The vector $\tilde{\mathbf{c}}$ in (6) contains the last $L_\mathrm{h} - 1$ samples of the STF, and $\mathbf{w}$ in (4) is a vector of additive white Gaussian noise (AWGN) with $w_i \sim \mathcal{CN}(0, \sigma_w^2)$. Since the eighth block of the CEF is equal to the last block of the STF, and $L_\mathrm{b} = 128$ is a multiple of the $\pi/2$ rotation period, (6) can be rewritten as

$$\tilde{\mathbf{c}} = [\, c_{\mathrm{CEF}_0} \;\; c_{\mathrm{CEF}_{8L_\mathrm{b}-1}} \;\; c_{\mathrm{CEF}_{8L_\mathrm{b}-2}} \;\cdots\; c_{\mathrm{CEF}_{8L_\mathrm{b}-(L_\mathrm{h}-1)}} \,]. \tag{7}$$

Therefore, $\mathbf{h}$ in (4) can be estimated by compensating for $\mathbf{C}$ in (5), which contains only CEF samples.

2.2 Data Part

Concerning the data part after the preamble, modulation and coding schemes (MCS) from 1 to 12 use SC by combining low-density parity-check (LDPC) channel codes with phase-shift keying (PSK) and quadrature amplitude modulation (QAM) constellation mappings.

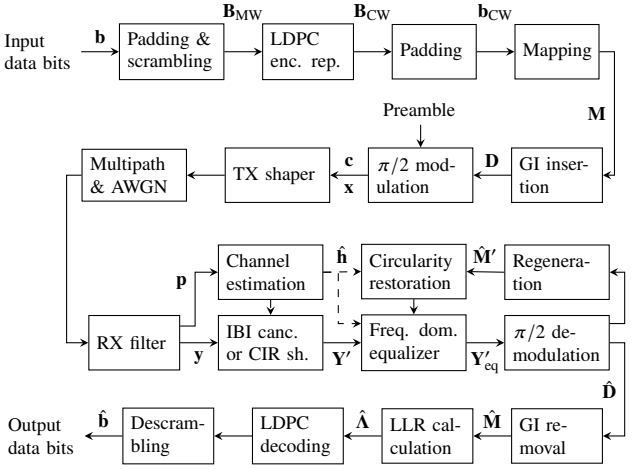

Fig. 2. Discrete-time model of the IEEE 802.11ad transmission and reception chain for data frames.

A model of the IEEE 802.11ad transmission chain for a data frame (physical layer service data unit) of L_PS information bytes is shown in the upper half of Fig. 2. Let us define the length of the LDPC codeword $L_\mathrm{CW} = 672$. Given the $8L_\mathrm{PS}$ information bits $\mathbf{b}$, the number of message words is $N_\mathrm{W} = \lceil 8L_\mathrm{PS}/L_\mathrm{MW} \rceil$, where $L_\mathrm{MW} = L_\mathrm{CW}r_\mathrm{C}/\rho$ is the message word length, and ρ is the repetition factor. When binary PSK (BPSK) with $r_\mathrm{C} = 1/2$ is used, the repetition factor can be either $\rho = 1$ (no repetition) or $\rho = 2$; in all other cases, only $\rho = 1$ is possible [3, p. 472]. In all the cases, the total code rate is r_C/ρ. The $8L_\mathrm{PS}$ information bits are padded with $L_\mathrm{DP} = N_\mathrm{W}L_\mathrm{MW} - 8L_\mathrm{PS}$ zeros, and scrambled by a binary sequence $\boldsymbol{\kappa}$ of length $N_\mathrm{W}L_\mathrm{MW}$, to obtain

$$\mathbf{b}_{\mathrm{SCR}} = \left(\begin{bmatrix} \mathbf{b} \\ \mathbf{0}_{L_\mathrm{DP}\times 1} \end{bmatrix} + \boldsymbol{\kappa} \right)_2. \tag{8}$$

Then, the scrambled bits are reshaped and padded into the $\rho L_\mathrm{MW} \times N_\mathrm{W}$ matrix whose columns contain the message words

$$\mathbf{B}_\mathrm{MW} = \begin{bmatrix} \mathrm{Unvec}_{L_\mathrm{MW},N_\mathrm{W}}(\mathbf{b}_{\mathrm{SCR}}) \\ \mathbf{0}_{(\rho-1)L_\mathrm{MW}\times N_\mathrm{W}} \end{bmatrix}, \tag{9}$$

where the matrix $\mathbf{0}_{(\rho-1)L_\mathrm{MW}\times N_\mathrm{W}}$ is empty in case of no repetition ($\rho = 1$). These bits are encoded with LDPC codes with rates from $r_\mathrm{C} = 1/2$ to $r_\mathrm{C} = 13/16$. When $\rho = 1$, the LDPC encoder produces the $L_\mathrm{CW} \times N_\mathrm{W}$ codeword matrix $\mathbf{B}_\mathrm{CW} = [\, \mathbf{B}_\mathrm{MW}^\mathrm{T} \; \mathbf{B}_\mathrm{PW}^\mathrm{T} \,]^\mathrm{T}$, where $\mathbf{B}_\mathrm{PW}$ contains the parity words. When $\rho = 2$, the LDPC encoder produces the $L_\mathrm{CW} \times N_\mathrm{W}$ codeword matrix

$$\mathbf{B}_\mathrm{CW} = \begin{bmatrix} \mathrm{Unvec}_{L_\mathrm{MW},N_\mathrm{W}}(\mathbf{b}_{\mathrm{SCR}}) \\ \mathrm{Unvec}_{L_\mathrm{MW},N_\mathrm{W}}((\mathbf{b}_{\mathrm{SCR}}+\bar{\boldsymbol{\kappa}})_2) \\ \mathbf{B}_\mathrm{PW} \end{bmatrix} \tag{10}$$

where $\bar{\boldsymbol{\kappa}}$ is another scrambling sequence of length $N_\mathrm{W}L_\mathrm{MW}$.

Let us define ν as the number of bits per symbol of the mapping, $L_\mathrm{CB} = \nu L_\mathrm{D}$ as the number of coded bits per block, with $L_\mathrm{D} = 448$, and $N_\mathrm{B} = \lceil N_\mathrm{W}L_\mathrm{CW}/L_\mathrm{CB} \rceil$ as the number of data blocks. Now, the encoded stream is formed as

[1] $N_\mathrm{S} = 17$ for data frames only; for control frames, $N_\mathrm{S} = 65$. In the OFDM mode, $\mathbf{S}_{\mathrm{CEF}}$ is slightly different from (2), as shown in [3, p. 450].

[2] Throughout this paper, we assume frequency synchronization and time synchronization, with a possible delay (the first taps of the CIR may be zero).

$$\mathbf{b}_{\mathrm{CW}} = \begin{bmatrix} \mathrm{vec}(\mathbf{B}_{\mathrm{CW}}) \\ \tilde{\boldsymbol{\kappa}} \end{bmatrix} \tag{11}$$

where $\tilde{\boldsymbol{\kappa}}$ is a pseudo-noise binary padding sequence of length $L_{\mathrm{BP}} = N_{\mathrm{B}}L_{\mathrm{CB}} - N_{\mathrm{W}}L_{\mathrm{CW}}$. At this point, mapping is performed using the ν columns of the matrix $\boldsymbol{\Lambda} = \mathrm{Unvec}_{\nu,N_{\mathrm{B}}L_{\mathrm{D}}}(\mathbf{b}_{\mathrm{CW}})^{\mathrm{T}}$, where $\nu = 1$ for BPSK (MCS1 through MCS5), $\nu = 2$ for quaternary PSK (QPSK) (MCS6 through MCS9), and $\nu = 4$ for 16QAM (MCS10 through MCS12). The mapped symbol vector for BPSK is given by

$$\boldsymbol{\mu} = 2\boldsymbol{\lambda}_0 - 1, \tag{12}$$

for QPSK it is given by

$$\boldsymbol{\mu} = \tfrac{\exp(-\mathrm{j}\frac{\pi}{4})}{\sqrt{2}}((2\boldsymbol{\lambda}_0 - 1) + \mathrm{j}(2\boldsymbol{\lambda}_1 - 1)), \tag{13}$$

and for 16QAM it is

$$\begin{aligned}\boldsymbol{\mu} = {} & \tfrac{1}{\sqrt{10}}((4\boldsymbol{\lambda}_0 - 2) - (2\boldsymbol{\lambda}_0 - 1)(2\boldsymbol{\lambda}_1 - 1)) \\ & + \tfrac{\mathrm{j}}{\sqrt{10}}((4\boldsymbol{\lambda}_2 - 2) - (2\boldsymbol{\lambda}_2 - 1)(2\boldsymbol{\lambda}_3 - 1)).\end{aligned} \tag{14}$$

Note that the symbol vector $\boldsymbol{\mu}$ includes all the symbols obtained from a single LDPC codeword. This vector is subsequently split in N_{B} blocks of length $L_{\mathrm{D}} = 448$, as expressed by $\mathbf{M} = \mathrm{Unvec}_{L_{\mathrm{D}},N_{\mathrm{B}}}(\boldsymbol{\mu})$, which is the matrix containing the N_{B} data blocks. Next, a known GI of $L_{\mathrm{G}} = 64$ symbols is periodically inserted between useful data blocks of $L_{\mathrm{D}} = 448$ symbols, to obtain blocks of $L_{\mathrm{B}} = L_{\mathrm{D}} + L_{\mathrm{G}} = 512$ symbols with a cyclic property. We denote the known GI with $\boldsymbol{\gamma}_{\mathrm{a}}$, which is a GS (called Ga_{64} in [3]) of length $L_{\mathrm{G}} = 64$. Hence, the matrix containing the data blocks becomes $\mathbf{D} = [\,\mathbf{M}^{\mathrm{T}}\ \boldsymbol{\Gamma}_{\mathrm{a}}^{\mathrm{T}}\,]^{\mathrm{T}}$, where $\boldsymbol{\Gamma}_{\mathrm{a}} = \mathbf{1}_{1\times N_{\mathrm{B}}} \otimes \boldsymbol{\gamma}_{\mathrm{a}}$ contains the inserted GI vectors. Since all the blocks of length L_{B} share the same final part of length L_{G}, each GI can be interpreted as the CP of the subsequent block of length L_{B}. Finally, $\pi/2$ rotation is performed, to obtain the generated signal of $L_{\mathrm{x}} = N_{\mathrm{B}}L_{\mathrm{B}} + L_{\mathrm{G}}$ samples

$$\mathbf{x} = \mathbf{R}_{L_{\mathrm{x}}} \begin{bmatrix} \boldsymbol{\gamma}_{\mathrm{a}} \\ \mathrm{vec}(\mathbf{D}) \end{bmatrix} \tag{15}$$

where, before rotation, the GI $\boldsymbol{\gamma}_{\mathrm{a}}$ is inserted also at the beginning of the whole stream $\mathrm{vec}(\mathbf{D})$ of all data blocks. The symbol stream $\mathbf{x}$ is then transmitted at the nominal *chip* rate of $F_{\mathrm{C}} = \frac{2}{3}2640 = 1760$ Msample/s.

The received signal corresponding to the data part, with size $L_{\mathrm{y}} = L_{\mathrm{x}} + L_{\mathrm{h}} - 1$, can be expressed as

$$\mathbf{y} = \mathbf{H}\mathbf{x} + \mathbf{w} \tag{16}$$

where $\mathbf{H} = \mathrm{Toep}([\,\mathbf{h}^{\mathrm{T}}\ \mathbf{0}_{1\times(L_{\mathrm{x}}-1)}\,]^{\mathrm{T}}; [\,h_0\ \mathbf{0}_{1\times(L_{\mathrm{x}}-1)}\,])$, and $\mathbf{w}$ is the AWGN of L_{y} samples. In (16) we have omitted the multipath interference from the header part to the data part: we assume that the header has been regenerated without errors and subtracted. However, the IBI due to the data is included, because the vector $\mathbf{x}$ includes the whole data stream that includes all the N_{B} blocks.

3. Channel Estimation

Several methods have been proposed for IEEE 802.11ad channel estimation. After a review of the existing methods, we propose two new channel estimation methods: a first one, based on the knowledge of the channel sparsity, and a second one, based on weighted MMSE estimation.

3.1 Existing Schemes

The first existing channel estimation method applies the pseudo-inverse (PI) of (5) to (4) obtain

$$\hat{\mathbf{h}}_{\mathrm{PI}} = \hat{\mathbf{C}}^{+}\mathbf{p} = (\hat{\mathbf{C}}^{\mathrm{H}}\hat{\mathbf{C}})^{-1}\hat{\mathbf{C}}^{\mathrm{H}}\mathbf{p} \tag{17}$$

where $\hat{\mathbf{C}}$ is defined as in (5)–(6) but with $L_{\mathrm{h}} = L_{\mathrm{b}} = 128$. This method is a standard way to estimate a channel, which is valid for several training-based schemes [35–37], including IEEE 802.11ad. For instance, the inversion method in [8] is based on (17) for channel estimation. A variant of the previous method extends the PI also to the STF part, as

$$\hat{\mathbf{h}}_{\mathrm{STF}} = \mathbf{C}'^{+}\mathbf{p}' \tag{18}$$

where $\mathbf{C}'$ of size $(N_{\mathrm{S}} + N_{\mathrm{b}})L_{\mathrm{b}} \times L_{\mathrm{b}}$ is defined similarly to $\mathbf{C}$ in (5), with the difference that it uses all the samples from the STF and CEF parts ($N_{\mathrm{S}} + N_{\mathrm{b}} = 26$ blocks), and $\mathbf{p}'$ is a longer version of $\mathbf{p}$ comprising also the STF part. Since (18) exploits also the STF, better performance is expected with respect to (17). However, the use of STF requires higher memory and produces an output with larger latency.

A second existing method uses the long cross-correlation (LXC) between the received signal and the transmitted CEF. Since the CEF is formed with several GSs [3], with good correlation properties, the cross-correlation between the received and transmitted signals should produce an estimate of the CIR. The LXC estimate is given by

$$\hat{\mathbf{h}}_{\mathrm{LXC}} = \tfrac{1}{N_{\mathrm{b}}L_{\mathrm{b}}}\hat{\mathbf{C}}^{\mathrm{H}}\mathbf{p}. \tag{19}$$

This estimation method is a low-complexity approximation of PI in (17), and does not fully exploit the pairwise complementary property of GSs.

A third existing method uses short cross-correlations (SXC) with the GSs and successive combining to exploit the complementary property of the GS [11], [34]. If we define the $N_{\mathrm{b}}L_{\mathrm{b}} \times N_{\mathrm{b}}L_{\mathrm{b}}$ Toeplitz matrices

$$\mathbf{G}_{\mathrm{a}} = \mathrm{Toep}([\,\mathbf{g}_{\mathrm{a}}^{\mathrm{T}}\ \mathbf{0}_{1\times(N_{\mathrm{b}}-1)L_{\mathrm{b}}}\,]^{\mathrm{T}}; [\,g_{\mathrm{a}0}\ \mathbf{0}_{1\times(N_{\mathrm{b}}L_{\mathrm{b}}-1)}\,]), \tag{20a}$$

$$\mathbf{G}_{\mathrm{b}} = \mathrm{Toep}([\,\mathbf{g}_{\mathrm{b}}^{\mathrm{T}}\ \mathbf{0}_{1\times(N_{\mathrm{b}}-1)L_{\mathrm{b}}}\,]^{\mathrm{T}}; [\,g_{\mathrm{b}0}\ \mathbf{0}_{1\times(N_{\mathrm{b}}L_{\mathrm{b}}-1)}\,]), \tag{20b}$$

and the $L_{\mathrm{b}} \times N_{\mathrm{b}}L_{\mathrm{b}}$ combining matrices

$$\mathbf{J}_{\mathrm{a}} = [\,0\ {-1}\ 0\ {-1}\ 0\ {+1}\ 0\ {-1}\ 0\,] \otimes \mathbf{I}_{L_{\mathrm{b}}}, \tag{21a}$$

$$\mathbf{J}_{\mathrm{b}} = [\,{-1}\ 0\ {+1}\ 0\ {-1}\ 0\ {-1}\ 0\ 0\,] \otimes \mathbf{I}_{L_{\mathrm{b}}}, \tag{21b}$$

the CIR of the SXC estimation method can be expressed as

$$\hat{\mathbf{h}}_{\mathrm{SXC}} = \tfrac{1}{(N_{\mathrm{b}}-1)L_{\mathrm{b}}}(\mathbf{J}_{\mathrm{a}}\mathbf{G}_{\mathrm{a}}^{\mathrm{H}} + \mathbf{J}_{\mathrm{b}}\mathbf{G}_{\mathrm{b}}^{\mathrm{H}})\mathbf{p}. \tag{22}$$

3.2 Proposed Schemes

To improve the IEEE 802.11ad channel estimation, we propose a new method that assumes a sparse channel and performs a sparse PI (SPI). The proposed method uses an initial estimate $\hat{\mathbf{h}}_{\mathrm{IN}}$ of the CIR, obtained with either (17), or (19), or (22), and a successive refined estimation of the largest taps only. The SPI method finds the $L_{\mathrm{s}} \leq L_{\mathrm{h}} \leq 128$ positions of the largest taps of $\hat{\mathbf{h}}_{\mathrm{IN}}$ and constructs a selection matrix $\mathbf{E}$ of size $L_{\mathrm{s}} \times L_{\mathrm{h}}$, whose ith row has a single 1 in the position of the ith selected tap of $\hat{\mathbf{h}}_{\mathrm{IN}}$, and 0 in the remaining $L_{\mathrm{h}} - 1$ positions. If $\mathbf{h}' = \mathbf{E}\mathbf{h}$ contains the taps in the L_{s} selected positions, then

$$\mathbf{h} = \mathbf{E}^{\mathrm{T}}\mathbf{h}' + \hat{\boldsymbol{\varepsilon}} = \mathbf{E}^{\mathrm{T}}\mathbf{E}\mathbf{h} + \hat{\boldsymbol{\varepsilon}} \tag{23}$$

where $\hat{\boldsymbol{\varepsilon}}$ is the error caused by approximating $\mathbf{h}$ with $\mathbf{E}^{\mathrm{T}}\mathbf{h}'$. If we substitute (23) in (4) and estimate $\mathbf{h}'$ by the pseudo-inverse as $\hat{\mathbf{h}}' = (\mathbf{C}\mathbf{E}^{\mathrm{T}})^{+}\mathbf{p}$, we obtain the SPI estimate

$$\hat{\mathbf{h}}_{\mathrm{SPI}} = \mathbf{E}^{\mathrm{T}}\hat{\mathbf{h}}' = \mathbf{E}^{\mathrm{T}}(\mathbf{E}\mathbf{C}^{\mathrm{H}}\mathbf{C}\mathbf{E}^{\mathrm{T}})^{-1}\mathbf{E}\mathbf{C}^{\mathrm{H}}\mathbf{p}. \tag{24}$$

The second proposed method uses sparsity and MMSE (SMS) estimation. We approximate the cross-correlation matrix of MMSE with $\hat{\mathbf{U}}_{\mathrm{IN}} = \mathrm{Diag}(\hat{\mathbf{h}}_{\mathrm{IN}}^{*} \odot \hat{\mathbf{h}}_{\mathrm{IN}})$, which gives higher importance to the highest channel taps. This is used together with $\mathbf{E}$ to select the highest taps only. The resulting SMS CIR estimate is

$$\hat{\mathbf{h}}_{\mathrm{SMS}} = \hat{\mathbf{U}}_{\mathrm{IN}}(\mathbf{C}\mathbf{E}^{\mathrm{T}})^{\mathrm{H}}(\mathbf{C}\mathbf{E}^{\mathrm{T}}\hat{\mathbf{U}}_{\mathrm{IN}}(\mathbf{C}\mathbf{E}^{\mathrm{T}})^{\mathrm{H}} + k_{\mathrm{u}}\sigma_w^2\mathbf{I}_{N_{\mathrm{b}}L_{\mathrm{b}}})^{-1}\mathbf{p} \tag{25a}$$

$$= \tfrac{1}{k_{\mathrm{u}}\sigma_w^2}\mathbf{E}^{\mathrm{T}}[\mathbf{I}_{L_{\mathrm{s}}} - \boldsymbol{\Gamma}\mathbf{C}\mathbf{E}^{\mathrm{T}}(\boldsymbol{\Gamma}\mathbf{C}\mathbf{E}^{\mathrm{T}} + k_{\mathrm{u}}\sigma_w^2\mathbf{I}_{L_{\mathrm{s}}})^{-1}]\boldsymbol{\Gamma}\mathbf{p} \tag{25b}$$

where $\boldsymbol{\Gamma} = \mathbf{E}\hat{\mathbf{U}}_{\mathrm{IN}}\mathbf{C}^{\mathrm{H}}$ and k_{u} is an amplification factor that (in absence of error modeling) should be 1, but it will be empirically optimized. Although they are equivalent [38], the SMS expression (25b) inverts a matrix of size $L_{\mathrm{s}} < L_{\mathrm{b}}$ and hence its complexity is greatly reduced with respect to the SMS expression (25a), where the matrix inverse has size $N_{\mathrm{b}}L_{\mathrm{b}} = 9L_{\mathrm{b}}$.

For both the SPI and SMS methods, a different choice of $\mathbf{E}$ leads to different cases, such as:

1. if $L_{\mathrm{s}} = L_{\mathrm{b}}$ and $\mathbf{E} = \mathbf{I}_{L_{\mathrm{s}}}$, then all channel taps are selected, and sparsity is not exploited;
2. if $L_{\mathrm{s}} < L_{\mathrm{b}}$ sparsity is exploited, guessing the order L_{s}, for instance, based on a threshold;
3. if $L_{\mathrm{s}} = \|\mathbf{h}\|_0$, we have a *partial genie-aided* estimation, where the sparsity order is known, but the positions of the largest taps are unknown;
4. if $L_{\mathrm{s}} = \|\mathbf{h}\|_0$ and $E_{i,n_i} = 1$, the receiver knows the exact positions of the nonzero taps, so we have a *full genie-aided* case.

4. Detection

The channel estimation methods described in Sec. 3.2 find a CIR with $L_{\mathrm{b}} = 128$ taps: since a GI of $L_{\mathrm{G}} = 64$ samples is insufficient for a CIR with $L_{\mathrm{h}} > L_{\mathrm{G}}+1 = 65$ taps, IBI from the previous block on the current block might arise. The proposed receiver uses MMSE diagonal frequency equalization with IBI cancellation, followed by restoration of circularity. An update of the LLR calculation is also proposed with the aim of improved LDPC decoding.

4.1 Equalization

First, from (16) we obtain

$$\mathbf{Y} = \mathrm{Unvec}_{L_{\mathrm{B}},N_{\mathrm{B}}}([\,\mathbf{0}_{L_{\mathrm{G}}}\ \mathbf{I}_{N_{\mathrm{B}}L_{\mathrm{B}}}\ \mathbf{0}_{N_{\mathrm{B}}L_{\mathrm{B}}\times(L_{\mathrm{h}}-1)}\,]\mathbf{y}), \tag{26a}$$

$$\mathbf{X} = \mathrm{Unvec}_{L_{\mathrm{B}},N_{\mathrm{B}}}([\,\mathbf{0}_{L_{\mathrm{G}}}\ \mathbf{I}_{N_{\mathrm{B}}L_{\mathrm{B}}}\,]\mathbf{x}), \tag{26b}$$

$$\mathbf{W} = \mathrm{Unvec}_{L_{\mathrm{B}},N_{\mathrm{B}}}([\,\mathbf{0}_{L_{\mathrm{G}}}\ \mathbf{I}_{N_{\mathrm{B}}L_{\mathrm{B}}}\ \mathbf{0}_{N_{\mathrm{B}}L_{\mathrm{B}}\times(L_{\mathrm{h}}-1)}\,]\mathbf{w}), \tag{26c}$$

$$\mathbf{y}_i = \mathbf{H}_{\mathrm{rd}}\begin{bmatrix}\mathbf{x}_{i-1}\\ \mathbf{x}_i\end{bmatrix} + \mathbf{w}_i, \tag{26d}$$

$$\mathbf{x}_i = \mathbf{R}_{L_{\mathrm{B}}}\begin{bmatrix}\boldsymbol{\mu}_{\mathrm{i}}\\ \boldsymbol{\gamma}_{\mathrm{a}}\end{bmatrix} \tag{26e}$$

where $\mathbf{y}_i$, $\mathbf{x}_i$, and $\mathbf{w}_i$ are the ith columns of $\mathbf{Y}$, $\mathbf{X}$, and $\mathbf{W}$, respectively, and the reduced-size channel matrix is $\mathbf{H}_{\mathrm{rd}} = \mathrm{Toep}(\mathbf{0}_{L_{\mathrm{B}}\times 1}; [\,\mathbf{0}_{1\times(L_{\mathrm{B}}-L_{\mathrm{h}}+1)}\ h_{L_{\mathrm{h}}-1}\ \cdots\ h_1\ h_0\ \mathbf{0}_{1\times(L_{\mathrm{B}}-1)}\,])$.

The vector $[\,\mathbf{x}_{i-1}^{\mathrm{T}}\ \mathbf{x}_i^{\mathrm{T}}\,]^{\mathrm{T}}$ in (26d) is equal to the vector $\mathbf{R}_{2L_{\mathrm{B}}}[\,\boldsymbol{\mu}_{i-1}^{\mathrm{T}}\ \boldsymbol{\gamma}_{\mathrm{a}}^{\mathrm{T}}\ \boldsymbol{\mu}_i^{\mathrm{T}}\ \boldsymbol{\gamma}_{\mathrm{a}}^{\mathrm{T}}\,]^{\mathrm{T}}$, hence the GI $\boldsymbol{\gamma}_{\mathrm{a}}$ plays the double role of known data symbols of the ith block $\mathbf{x}_i$ and CP for the same ith block: this means that the linear convolution with the channel can be considered cyclic. Thus, we can define a single-tap frequency domain equalizer $\mathbf{q}$ of size $L_{\mathrm{B}} \times 1$ that provides the equalized signal

$$\mathbf{y}_{\mathrm{eq}_i} = \mathbf{F}^{\mathrm{H}}\,\mathrm{Diag}(\mathbf{q})\mathbf{F}\mathbf{y}_i \tag{27}$$

where $\mathbf{F}$ is the normalized DFT matrix of size L_{B}. In the zero-forcing (ZF) case, the equalizer becomes

$$\mathbf{q} = \mathrm{Diag}(\hat{\mathbf{h}}_{\mathrm{f}})^{-1}\mathbf{1}_{L_{\mathrm{B}}\times 1} \tag{28}$$

where $\hat{\mathbf{h}}_{\mathrm{f}} = \mathbf{F}\hat{\mathbf{h}}$, while, in the MMSE case, the equalizer is

$$\mathbf{q} = k_{\mathrm{MS}}\,\mathrm{Diag}(\hat{\mathbf{h}})^{\mathrm{H}}(\hat{\mathbf{U}} + \sigma_w^2\mathbf{I}_{L_{\mathrm{B}}})^{-1}\mathbf{1}_{L_{\mathrm{B}}\times 1} \tag{29}$$

where $\hat{\mathbf{U}} = \mathrm{Diag}(\hat{\mathbf{h}}^{*} \odot \hat{\mathbf{h}})$ and $k_{\mathrm{MS}} = \frac{1}{L_{\mathrm{B}}}\,\mathrm{tr}(\hat{\mathbf{U}}(\hat{\mathbf{U}} + \sigma_w^2\mathbf{I}_{L_{\mathrm{B}}})^{-1})$. From (27) we retrieve the information data part (after de-rotation and GI removal) with

$$\hat{\boldsymbol{\mu}}_i = \left[\,\mathbf{R}_{L_{\mathrm{D}}}^{\mathrm{H}}\ \mathbf{0}_{L_{\mathrm{D}}\times L_{\mathrm{G}}}\,\right]\mathbf{y}_{\mathrm{eq}_i}. \tag{30}$$

For instance, ZF single-tap frequency-domain equalization is employed in [11], while [12] compares both ZF and MMSE equalizers. However, none of these works include IBI cancellation.

4.2 Proposed IBI Cancellation

If $L_{\mathrm{h}} < L_{\mathrm{b}} + 1 = 129$, the following steps are needed to correctly subtract IBI from the previous $(i-1)$th block and to restore circularity by adding intersymbol interference (ISI) on the current ith block (see an example in Fig. 3):

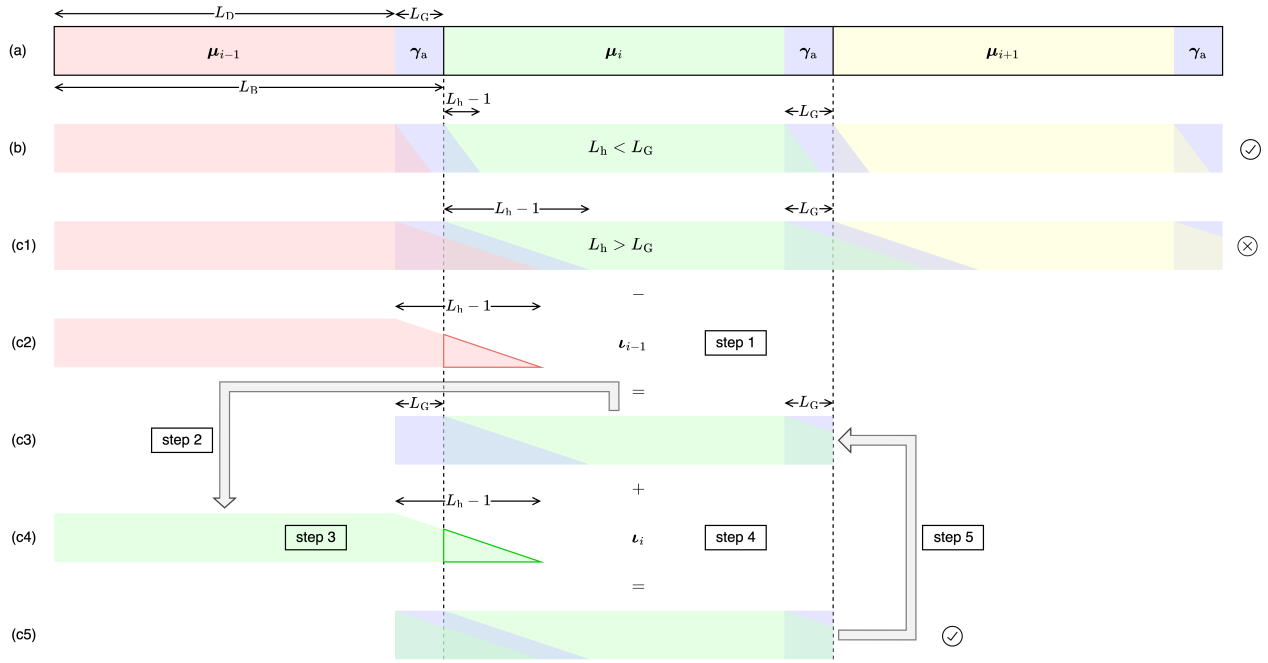

Fig. 3. Exemplification of IBI cancellation and circularity restoration (for simplicity, $\pi/2$ rotation is omitted): (a) transmitted data stream; (b) received data stream when the CIR is shorter than the GI, no IBI is present; (c1) received data stream when the CIR is longer than the GI, IBI is present; (c2) subtraction of IBI due to the previous block; (c3) current block with cancelled IBI; (c4) circularity restoration by addition of the ISI due to the current block; (c5) current block with cancelled IBI and restored circularity.

1. **IBI subtraction and first equalization:** assuming to have estimated the data $\hat{\boldsymbol{\mu}}'_{i-1}$ of the previous block, we subtract the IBI $\boldsymbol{\iota}_{i-1}$ generated by the previous block (to create an IBI-free current data block) and we go through the equalization process, using (27) with (28) or (29). The equalized data block $\mathbf{y}_{\mathrm{eq}_i}$, the IBI-free data block $\mathbf{y}'_i$, and the IBI $\boldsymbol{\iota}_{i-1}$, are expressed by

$$\mathbf{y}_{\mathrm{eq}_i} = \mathbf{F}^{\mathrm{H}}\,\mathrm{Diag}(\mathbf{q})\mathbf{F}\mathbf{y}'_i, \tag{31}$$

$$\mathbf{y}'_i = \mathbf{y}_i - \boldsymbol{\iota}_{i-1}, \tag{32}$$

$$\boldsymbol{\iota}_{i-1} = \mathbf{H}_{\mathrm{rd}} \begin{bmatrix} \mathbf{R}_{L_{\mathrm{D}}} \\ \mathbf{0}_{(2L_{\mathrm{B}}-L_{\mathrm{D}})\times L_{\mathrm{D}}} \end{bmatrix} \hat{\boldsymbol{\mu}}'_{i-1}. \tag{33}$$

For the block $i = 0$, we use $\boldsymbol{\iota}_{-1}$ obtained from the header.

2. **Data regeneration:** we regenerate the data in the current block, so as to use them for interference calculation. We first select the informative part of $\mathbf{y}_{\mathrm{eq}_i}$ by applying (30), and we decide the symbols according to the used modulation. For BPSK, the regenerated data are

$$\hat{\mu}'_{i,n} = \mathrm{sgn}\,\mathrm{Re}(\hat{\mu}_{i,n}), \tag{34}$$

while for QPSK they are

$$\hat{\mu}'_{i,n} = \frac{\exp(-\mathrm{j}\frac{\pi}{4})}{\sqrt{2}}\,\mathrm{sgn}\,\mathrm{Re}(\sqrt{2}\exp(\mathrm{j}\tfrac{\pi}{4})\hat{\mu}_{i,n}) + \mathrm{j}\frac{\exp(-\mathrm{j}\frac{\pi}{4})}{\sqrt{2}}\,\mathrm{sgn}\,\mathrm{Im}(\sqrt{2}\exp(\mathrm{j}\tfrac{\pi}{4})\hat{\mu}_{i,n}), \tag{35}$$

and for 16QAM they are

$$\hat{\mu}'_{i,n} = \frac{\mathrm{sgn}\,\mathrm{Re}(\sqrt{10}\hat{\mu}_{i,n})}{\sqrt{10}}(2+\mathrm{sgn}(|\,\mathrm{Re}(\sqrt{10}\hat{\mu}_{i,n})|-2)) + \mathrm{j}\frac{\mathrm{sgn}\,\mathrm{Im}(\sqrt{10}\hat{\mu}_{i,n})}{\sqrt{10}}(2+\mathrm{sgn}(|\,\mathrm{Im}(\sqrt{10}\hat{\mu}_{i,n})|-2)). \tag{36}$$

3. **IBI/ISI calculation:** we calculate the interference from the regenerated data as

$$\boldsymbol{\iota}_i = \mathbf{H}_{\mathrm{rd}} \begin{bmatrix} \mathbf{R}_{L_{\mathrm{D}}} \\ \mathbf{0}_{(2L_{\mathrm{B}}-L_{\mathrm{D}})\times L_{\mathrm{D}}} \end{bmatrix} \hat{\boldsymbol{\mu}}'_i. \tag{37}$$

The vector $\boldsymbol{\iota}_i$ will be used to recreate the ISI for the current block i and the IBI for the following block $i+1$.

4. **Circularity restoration:** to enable low-complexity diagonal equalization in the frequency domain, we add the ISI to the current data block, so that circularity is restored. Then, we re-apply the equalizer to the current block, which has now no IBI, as

$$\mathbf{y}'_{\mathrm{eq}_i} = \mathbf{F}^{\mathrm{H}}\,\mathrm{Diag}(\mathbf{q})\mathbf{F}(\mathbf{y}'_i + \boldsymbol{\iota}_i) = \mathbf{y}_{\mathrm{eq}_i} + \mathbf{F}^{\mathrm{H}}\,\mathrm{Diag}(\mathbf{q})\mathbf{F}\boldsymbol{\iota}_i. \tag{38}$$

5. **Iterative refinement:** if further errors are still expected, repeat the steps 1–2–3–4 for $N_{\mathrm{IT}} - 1$ times.

4.3 Channel Shortening

As an alternative to IBI cancellation, the CIR shortening technique can be adopted [29–32]. Here, we summarize an existing CIR shortening solution to compare with our proposed IBI canceler. With CIR shortening, a finite-impulse response (FIR) filter is inserted before channel equalization: this FIR filter, with response $\mathbf{v}$ of length L_v, extends the actual duration L_h of the CIR, but also concentrates its energy within the first L_G samples, so that IBI is almost entirely eliminated. The filter $\mathbf{v}$ can be designed with the maximum shortening SNR method [29–32], aiming at maximizing the signal-to-IBI ratio. We define the shortened CIR of length $L_\mathrm{sh} = L_\mathrm{h} + L_\mathrm{v} - 1$ as

$$\mathbf{h}_\mathrm{sh} = \tilde{\mathbf{H}}\mathbf{v}, \tag{39}$$

$$\tilde{\mathbf{H}} = \mathrm{Toep}(\left[\begin{array}{cc}\mathbf{h}^\mathrm{T} & \mathbf{0}_{1\times(L_\mathrm{v}-1)}\end{array}\right]^\mathrm{T}; \left[\begin{array}{cc}h_0 & \mathbf{0}_{1\times(L_\mathrm{v}-1)}\end{array}\right]). \tag{40}$$

The method maximizes the ratio

$$\frac{\|\boldsymbol{\Sigma}_\mathrm{in}\mathbf{h}_\mathrm{sh}\|^2}{\|\boldsymbol{\Sigma}_\mathrm{out}\mathbf{h}_\mathrm{sh}\|^2} = \frac{\|\boldsymbol{\Sigma}_\mathrm{in}\tilde{\mathbf{H}}\mathbf{v}\|^2}{\|\boldsymbol{\Sigma}_\mathrm{out}\tilde{\mathbf{H}}\mathbf{v}\|^2} \tag{41}$$

of the energies of the shortened CIR inside and outside a window of length L_in, where

$$\boldsymbol{\Sigma}_\mathrm{in} = \left[\begin{array}{ccc}\mathbf{0}_{L_\mathrm{in}\times\Delta} & \mathbf{I}_{L_\mathrm{in}} & \mathbf{0}_{L_\mathrm{in}\times L_\mathrm{out}}\end{array}\right], \tag{42a}$$

$$\boldsymbol{\Sigma}_\mathrm{out} = \left[\begin{array}{ccc}\mathbf{I}_\Delta & \mathbf{0}_{\Delta\times L_\mathrm{in}} & \mathbf{0}_{\Delta\times L_\mathrm{out}} \\ \mathbf{0}_{L_\mathrm{out}\times\Delta} & \mathbf{0}_{L_\mathrm{out}\times L_\mathrm{in}} & \mathbf{I}_{L_\mathrm{out}}\end{array}\right], \tag{42b}$$

Δ and L_in are design parameters, and $L_\mathrm{out} = L_\mathrm{sh} - L_\mathrm{in} - \Delta$. By defining $\mathbf{A}_\mathrm{in} = \tilde{\mathbf{H}}^\mathrm{H}\boldsymbol{\Sigma}_\mathrm{in}^\mathrm{H}\boldsymbol{\Sigma}_\mathrm{in}\tilde{\mathbf{H}}$ and $\mathbf{A}_\mathrm{out} = \tilde{\mathbf{H}}^\mathrm{H}\boldsymbol{\Sigma}_\mathrm{out}^\mathrm{H}\boldsymbol{\Sigma}_\mathrm{out}\tilde{\mathbf{H}}$, the maximization of the ratio in (41) corresponds to the minimization of $\mathbf{v}^\mathrm{H}\mathbf{A}_\mathrm{out}\mathbf{v}$ subject to $\mathbf{v}^\mathrm{H}\mathbf{A}_\mathrm{in}\mathbf{v} = 1$ [29]. Therefore, this criterion minimizes the IBI for a useful signal with unit energy. The solution $\mathbf{v}$ can be found by calculating the generalized eigenvectors of the matrices $\mathbf{A}_\mathrm{out}$ and $\mathbf{A}_\mathrm{in}$, and selecting the generalized eigenvector corresponding to the minimum generalized eigenvalue.

After channel shortening, the filtered received signal is expressed by

$$\mathbf{y}'_\mathrm{sh} = \mathbf{V}\mathbf{y} \tag{43}$$

where $\mathbf{V} = \mathrm{Toep}(\left[\begin{array}{cc}\mathbf{v}^\mathrm{T} & \mathbf{0}_{1\times(L_\mathrm{y}-1)}\end{array}\right]^\mathrm{T}; \left[\begin{array}{cc}v_0 & \mathbf{0}_{1\times(L_\mathrm{y}-1)}\end{array}\right])$. In this case, the MMSE equalizer (29) is modified as

$$\mathbf{q} = k_\mathrm{sh}\,\mathrm{Diag}(\hat{\mathbf{h}}_\mathrm{sh})^\mathrm{H}(\hat{\mathbf{U}}_\mathrm{sh} + \sigma_w^2\,\mathrm{Diag}((\tilde{\mathbf{F}}\mathbf{v})^*\odot(\tilde{\mathbf{F}}\mathbf{v}))^{-1}\mathbf{1}_{L_\mathrm{B}\times 1} \tag{44}$$

where $\hat{\mathbf{U}}_\mathrm{sh} = \mathrm{Diag}(\hat{\mathbf{h}}_\mathrm{sh}^*\odot\hat{\mathbf{h}}_\mathrm{sh})$, $k_\mathrm{sh} = \frac{1}{L_\mathrm{B}}\,\mathrm{tr}(\hat{\mathbf{U}}_\mathrm{sh}(\hat{\mathbf{U}}_\mathrm{sh} + \sigma_w^2\mathbf{F}\mathbf{v})^{-1})$, and $\hat{\mathbf{h}}_\mathrm{sh}$ is the estimated channel after shortening, obtained by filtering the estimate $\hat{\mathbf{h}}$ as in (39)–(40).

4.4 Proposed LLR Update

Here, we propose a simple method to estimate the amount of total noise and interference power at the input of the LDPC decoder, so as to provide the correct shapes for the LLR curves used in the soft-decision demapper. For the power calculations, we use the signal with IBI included, so that we can quantify also the IBI power. From (16), we obtain the ith noisy and interference-distorted signal block $\hat{\boldsymbol{\mu}}_i$, as

$$\begin{aligned}\hat{\boldsymbol{\mu}}_i &= \mathbf{N}_i\mathbf{y} = \mathbf{N}_i(\mathbf{H}\mathbf{x} + \mathbf{w}) = \mathbf{N}_i\mathbf{H}\mathbf{x} + \mathbf{N}_i\mathbf{w} \\ &= \mathbf{N}_i\mathbf{H}\mathbf{R}_{L_\mathrm{x}}\left[\begin{array}{c}\boldsymbol{\gamma}_\mathrm{a} \\ \mathrm{vec}\left(\left[\begin{array}{c}\mathbf{M} \\ \boldsymbol{\Gamma}_\mathrm{a}\end{array}\right]\right)\end{array}\right] + \mathbf{N}_i\mathbf{w} \\ &= \mathbf{Z}_i\left[\begin{array}{c}\boldsymbol{\gamma}_\mathrm{a} \\ \mathrm{vec}\left(\left[\begin{array}{c}\mathrm{Unvec}_{L_\mathrm{D},N_\mathrm{B}}(\boldsymbol{\mu}) \\ \mathbf{1}_{1\times N_\mathrm{B}}\otimes\boldsymbol{\gamma}_\mathrm{a}\end{array}\right]\right)\end{array}\right] + \mathbf{N}_i\mathbf{w} \\ &= \mathbf{B}_i\boldsymbol{\mu} + \mathbf{G}_i\boldsymbol{\gamma}_\mathrm{a} + \mathbf{N}_i\mathbf{w}\end{aligned} \tag{45}$$

where $\mathbf{Z}_i = \mathbf{N}_i\mathbf{H}\mathbf{R}_{L_\mathrm{x}}$, $\mathbf{N}_i = \left[\begin{array}{cc}\mathbf{R}_{L_\mathrm{D}}^\mathrm{H} & \mathbf{0}_{L_\mathrm{D}\times L_\mathrm{G}}\end{array}\right]\mathbf{F}^\mathrm{H}\mathrm{Diag}(\mathbf{q})\mathbf{F}\mathbf{K}_i\mathbf{V}$, and $\mathbf{K}_i = \left[\begin{array}{cccc}\mathbf{0}_{L_\mathrm{B}\times(L_\mathrm{G}+iL_\mathrm{B})} & \mathbf{I}_{L_\mathrm{B}} & \mathbf{0}_{L_\mathrm{B}\times(L_\mathrm{y}+L_\mathrm{v}-1-L_\mathrm{G}-(i+1)L_\mathrm{B})}\end{array}\right]$ selects the samples corresponding to the ith data block (i.e., it excludes the other blocks and the initial GI $\boldsymbol{\gamma}_\mathrm{a}$). The result $\hat{\boldsymbol{\mu}}_i$ in (45) contains three parts: $\mathbf{B}_i\boldsymbol{\mu}$ is the signal-plus-interference, $\mathbf{G}_i\boldsymbol{\gamma}_\mathrm{a}$ is the GI part, and $\mathbf{N}_i\mathbf{w}$ is the filtered noise. The relations among $\mathbf{Z}_i$, $\mathbf{B}_i$, and $\mathbf{G}_i$ are

$$\mathbf{Z}_i = \left[\begin{array}{ccccccccc}\mathbf{G}_{i,-1} & \mathbf{B}_{i,0} & \mathbf{G}_{i,0} & \cdots & \mathbf{B}_{i,i-1} & \mathbf{G}_{i,i-1} & \mathbf{B}_{i,i} & \mathbf{G}_{i,i} & \cdots\end{array}\right], \tag{46a}$$

$$\mathbf{B}_i = \left[\begin{array}{ccccc}\mathbf{B}_{i,0} & \cdots & \mathbf{B}_{i,i-1} & \mathbf{B}_{i,i} & \cdots\end{array}\right], \tag{46b}$$

$$\mathbf{G}_i = \textstyle\sum_{l=-1}^{i}\mathbf{G}_{i,l} \tag{46c}$$

where

$$\mathbf{B}_{i,l} = \mathbf{Z}_i\left[\begin{array}{c}\mathbf{0}_{(L_\mathrm{G}+lL_\mathrm{B})\times L_\mathrm{D}} \\ \mathbf{I}_{L_\mathrm{D}} \\ \mathbf{0}_{(L_\mathrm{x}-(l+1)L_\mathrm{B})\times L_\mathrm{D}}\end{array}\right] \tag{47}$$

and

$$\mathbf{G}_{i,l} = \mathbf{Z}_i\left[\begin{array}{c}\mathbf{0}_{(l+1)L_\mathrm{B}\times L_\mathrm{G}} \\ \mathbf{I}_{L_\mathrm{G}} \\ \mathbf{0}_{(L_\mathrm{x}-L_\mathrm{G}-(l+1)L_\mathrm{B})\times L_\mathrm{G}}\end{array}\right]. \tag{48}$$

In (47), $\mathbf{B}_{i,i}$ contains the useful signal and the ISI, $\mathbf{B}_{i,l}$ ($l \neq i$) represents the IBI of block lth on block ith, and $\mathbf{G}_i$ in (48) is the interference due to GIs. Considering a causal cascade of processing systems and $L_\mathrm{h} \leq L_\mathrm{B}$, we obtain $\mathbf{B}_{i,l} = \mathbf{0}_{L_\mathrm{D}\times L_\mathrm{D}}$ for $l \notin \{i, i-1\}$. Therefore, the signal (45) becomes

$$\hat{\boldsymbol{\mu}}_i = \underbrace{\mathbf{D}_{i,i}\boldsymbol{\mu}_i}_{\text{Useful}} + \underbrace{(\mathbf{B}_{i,i} - \mathbf{D}_{i,i})\boldsymbol{\mu}_i}_{\text{ISI}} + \underbrace{\mathbf{B}_{i,i-1}\boldsymbol{\mu}_{i-1}}_{\text{IBI}} + \underbrace{\mathbf{G}_i\boldsymbol{\gamma}_\mathrm{a}}_{\text{GI part}} + \underbrace{\mathbf{N}_i\mathbf{w}}_{\text{Noise}} \tag{49}$$

where $\mathbf{D}_{i,i} = \mathbf{B}_{i,i}\odot\mathbf{I}_{L_\mathrm{D}}$ is a matrix containing only the main diagonal of $\mathbf{B}_{i,i}$. From (49) we obtain the average power vector of the useful signal as

$$\mathbf{p}_\mathrm{S} = \mathrm{diag}(\mathbf{D}_{i,i}\mathbf{D}_{i,i}^\mathrm{H}), \tag{50}$$

the average power vector of the interference as

$$\begin{aligned}\mathbf{p}_\mathrm{I} &= \mathrm{diag}((\mathbf{B}_{i,i} - \mathbf{D}_{i,i})(\mathbf{B}_{i,i} - \mathbf{D}_{i,i})^\mathrm{H}) \\ &\quad + \mathrm{diag}(\mathbf{B}_{i,i-1}\mathbf{B}_{i,i-1}^\mathrm{H}) + \mathrm{diag}(\mathbf{G}_i\boldsymbol{\gamma}_\mathrm{a}\boldsymbol{\gamma}_\mathrm{a}^\mathrm{H}\mathbf{G}_i^\mathrm{H}),\end{aligned} \tag{51}$$

and the average power vector of the noise as

$$\mathbf{p}_\mathrm{N} = \sigma_w^2\,\mathrm{diag}(\mathbf{N}_{i,i}\mathbf{N}_{i,i}^\mathrm{H}). \tag{52}$$

In (51), the GI part $\mathrm{diag}(\mathbf{G}_i\boldsymbol{\gamma}_\mathrm{a}\boldsymbol{\gamma}_\mathrm{a}^\mathrm{H}\mathbf{G}_i^\mathrm{H})$ is negligible. When IBI cancellation is performed, the IBI component $\mathrm{diag}(\mathbf{B}_{i,i-1}\mathbf{B}_{i,i-1}^\mathrm{H})$ is absent in (51).

The equalized data block $\hat{\boldsymbol{\mu}}_i$ is the soft-input of the LDPC channel decoder: a soft demapper prepares the LLR matrix $\hat{\boldsymbol{\Lambda}}$ of size $\nu \times N_\mathrm{B} L_\mathrm{D}$ from matrix $\hat{\mathbf{M}}$, which holds the N_B data blocks $\hat{\boldsymbol{\mu}}_i$ as columns, knowing the useful, interference, and noise powers in (50)–(52). For LLR demapping, we assume that the interference is Gaussian, uncorrelated with both the useful signal and the noise, and that its power is equally split between real and imaginary components. Moreover, we normalize the signal by dividing it by $\sqrt{p_{\mathrm{S}_n}}$. Thus, the in-phase and quadrature noise components of the mapped signal have the same standard deviation

$$\sigma_n = \sqrt{\frac{p_{\mathrm{N}_n} + p_{\mathrm{I}_n}}{2 p_{\mathrm{S}_n}}}. \tag{53}$$

By defining k as the symbol index that spans the whole stream, the block index is $i = \lfloor k/L_\mathrm{D} \rfloor$ and the symbol index inside the block is $n = (k)_{L_\mathrm{D}}$. For the single-bit BPSK decoder, the entries of $\hat{\boldsymbol{\Lambda}}$ become

$$\hat{\lambda}_{0,k} = -2\,\mathrm{Re}(\hat{\mu}_{i,n}/\sqrt{p_{\mathrm{S}_n}})/\sigma_n^2, \tag{54}$$

for the QPSK decoder the entries of $\hat{\boldsymbol{\Lambda}}$ are

$$\hat{\lambda}_{0,k} = -2\,\mathrm{Re}(\exp(\mathrm{j}\tfrac{\pi}{4})\hat{\mu}_{i,n}/\sqrt{p_{\mathrm{S}_n}})/\sigma_n^2, \tag{55a}$$

$$\hat{\lambda}_{1,k} = -2\,\mathrm{Im}(\exp(\mathrm{j}\tfrac{\pi}{4})\hat{\mu}_{i,n}/\sqrt{p_{\mathrm{S}_n}})/\sigma_n^2, \tag{55b}$$

and for the 16QAM decoder [3] the entries are

$$\begin{aligned}\hat{\lambda}_{0,k} = \mathrm{lexp}\Bigg(&\frac{\left[\sqrt{\frac{10}{p_{\mathrm{S}_n}}}\,\mathrm{Re}(\hat{\mu}_{i,n})+3\right]^2}{20\sigma_n^2}, \frac{\left[\sqrt{\frac{10}{p_{\mathrm{S}_n}}}\,\mathrm{Re}(\hat{\mu}_{i,n})+1\right]^2}{20\sigma_n^2}\Bigg)\\ - \mathrm{lexp}\Bigg(&\frac{\left[\sqrt{\frac{10}{p_{\mathrm{S}_n}}}\,\mathrm{Re}(\hat{\mu}_{i,n})-1\right]^2}{20\sigma_n^2}, \frac{\left[\sqrt{\frac{10}{p_{\mathrm{S}_n}}}\,\mathrm{Re}(\hat{\mu}_{i,n})-3\right]^2}{20\sigma_n^2}\Bigg),\end{aligned} \tag{56a}$$

$$\begin{aligned}\hat{\lambda}_{1,k} = \mathrm{lexp}\Bigg(&\frac{\left[\sqrt{\frac{10}{p_{\mathrm{S}_n}}}\,\mathrm{Re}(\hat{\mu}_{i,n})+3\right]^2}{20\sigma_n^2}, \frac{\left[\sqrt{\frac{10}{p_{\mathrm{S}_n}}}\,\mathrm{Re}(\hat{\mu}_{i,n})-3\right]^2}{20\sigma_n^2}\Bigg)\\ - \mathrm{lexp}\Bigg(&\frac{\left[\sqrt{\frac{10}{p_{\mathrm{S}_n}}}\,\mathrm{Re}(\hat{\mu}_{i,n})-1\right]^2}{20\sigma_n^2}, \frac{\left[\sqrt{\frac{10}{p_{\mathrm{S}_n}}}\,\mathrm{Re}(\hat{\mu}_{i,n})+1\right]^2}{20\sigma_n^2}\Bigg)\end{aligned} \tag{56b}$$

where

$$\mathrm{lexp}(a, b) = \ln[\exp(-a) + \exp(-b)] \tag{57}$$

and $\hat{\lambda}_{2,k}$ and $\hat{\lambda}_{3,k}$ are obtained from (56) by replacing $\mathrm{Re}(\hat{\mu}_{i,n})$ with $\mathrm{Im}(\hat{\mu}_{i,n})$.

When repetition is used (MCS1, BPSK with $r_\mathrm{C} = 1/2$), at the receiver we combine the samples as

$$\tilde{\mu}_k = \frac{\hat{\mu}_{i,n} + (-1)^{\bar{\kappa}_l}\hat{\mu}_{i',n'}}{2} \tag{58}$$

to perform equal gain combining, where $\bar{\kappa}_l$ is the lth sample of the scrambling sequence $\bar{\boldsymbol{\kappa}}$, $l = (k)_{L_\mathrm{CW}}$, $i' = \lfloor (k+L_\mathrm{MW})/L_\mathrm{D} \rfloor$, and $n' = (k + L_\mathrm{MW})_{L_\mathrm{D}}$. Then, by repeating the same strategy done in (49)–(53), applied after the combining (58), we obtain the LLR expressed by

$$\hat{\lambda}_{0,k} = \begin{cases} -\frac{2\,\mathrm{Re}(\tilde{\mu}_k)}{\sqrt{\tilde{p}_{\mathrm{S}_k}}\,\tilde{\sigma}_k^2}, & 0 \le l < L_\mathrm{MW}, \\ +\infty, & L_\mathrm{MW} \le l < 2L_\mathrm{MW}, \\ -\frac{2\,\mathrm{Re}(\hat{\mu}_{i,n})}{\sqrt{p_{\mathrm{S}_n}}\,\sigma_n^2}, & 2L_\mathrm{MW} \le l < L_\mathrm{CW}, \end{cases} \tag{59}$$

where $\tilde{p}_{\mathrm{S}_k}$ and $\tilde{\sigma}_k^2$ are calculated as in (50)–(53) applied after combining (58).

The proposed LLR update (53)–(59) has been obtained by estimating the power p_{S_n} of the useful signal component, the power p_{I_n} of the interference, and the noise power p_{N_n}. However, the conventional LLR demapper [33] does not distinguish between the interference and the useful signal, and adopts an estimate of the signal power $p'_{\mathrm{S}_n} = p_{\mathrm{S}_n} + p_{\mathrm{I}_n}$, which includes the interference. Therefore, the conventional LLR computation uses a different expression of (53), that is

$$\sigma'_n = \sqrt{\frac{p_{\mathrm{N}_n}}{2p'_{\mathrm{S}_n}}}, \tag{60}$$

and normalizes by $\sqrt{p'_{\mathrm{S}_n}}$ instead of by $\sqrt{p_{\mathrm{S}_n}}$.

5. Simulation Results

The mathematical equations of Secs. 2–4 have been modeled in the MATLAB programming language (version R2022b) and simulated[3] on a Ubuntu OS PC with 128 Gbytes of RAM and a Intel i9 with 18-core CPU working at 3 GHz.

5.1 Channel Estimation Performance

We have simulated two different types of channel, and the CIR has been kept constant for the whole duration of the CEF. For the first type, the channel taps have been randomly generated according to an exponentially decaying power-delay profile, as

$$h_n = \sum_{i=0}^{S_\mathrm{C}-1} \eta_i \exp(-\tfrac{n_i}{100})\delta_{n-n_i}, \tag{61}$$

$n = 0, \ldots, L_\mathrm{h} - 1$, with unique $n_i \sim \mathcal{U}\{0, L_\mathrm{h} - 1\}$ and $\eta_i \sim \mathcal{CN}(0, 1)$. In (61), we have used $L_\mathrm{h} = 128$ and $S_\mathrm{C} = 20$. This type of channel intends to represent an outdoor situation with multiple isolated reflections. The second type is represented by the channel denoted as "*Scenario 1*" in [16], which uses a dataset measured by Brno University of Technology. The data span the frequencies from 55 GHz to 65 GHz and represent an indoor channel typical of a medium-sized office. The same channel can also be used for modeling the transmission of similar mmWave standards, such as the IEEE 802.11ay [17], which is the successor of IEEE 802.11ad. For our tests, we have converted the original sampling rate (10 Gsample/s) to our simulation sampling rate ($F_\mathrm{C} = 1.76$ Gsample/s) by adopting an equal-energy criterion in time, we have removed the initial low-energy samples, and we have truncated the obtained CIR to L_b taps. The estimators performance has been evaluated in terms of the normalized mean square error (NMSE)

[3] Part of the MATLAB code and operating instructions are available at https://github.com/gbaruffa/liquid-edge-ieee802.11ad-phy-public.

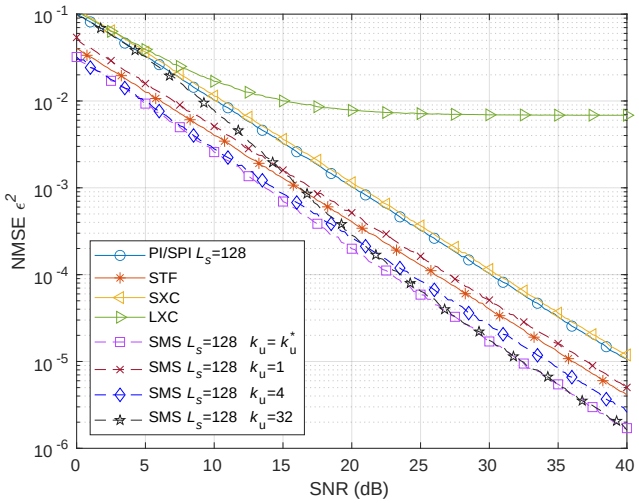

Fig. 4. NMSE of estimation methods for the channel (61).

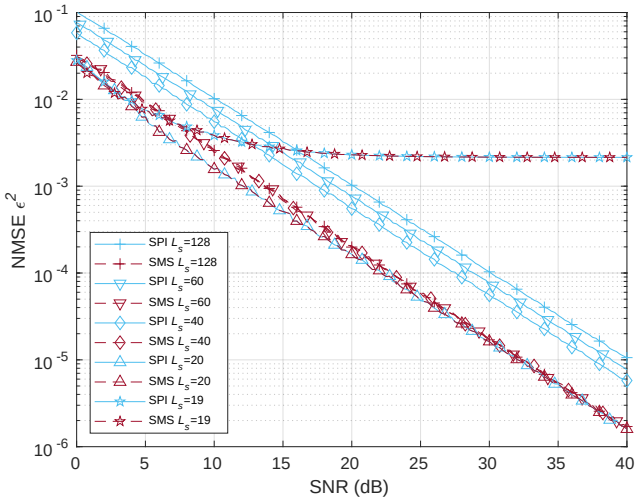

Fig. 5. NMSE of SPI and SMS methods for the channel (61).

$$\epsilon^2 = \frac{1}{N_{\text{est}}} \sum_{i=0}^{N_{\text{est}}-1} \frac{\|\hat{\mathbf{h}}_i - \mathbf{h}\|^2}{\|\mathbf{h}\|^2}, \tag{62}$$

averaged over $N_{\text{est}} = 100$ channel estimates $\hat{\mathbf{h}}_i$ for every SNR.

Figure 4 plots the NMSE of different estimators for the simulated channel (61) with $S_{\text{C}} = 20$ nonnull taps. All the estimators do not exploit sparsity ($L_{\text{s}} = L_{\text{b}} = 128$). The LXC method is the worst performer and produces an error floor, because this method does not exploit the complementary property of the GSs. Instead, the SXC method exploits this property and performs as expected. The SPI method with $L_{\text{s}} = 128$ coincides with the PI method and has performance close to that of SXC, with minor improvements, since both methods exploit also the last GS of the CEF ($\mathbf{g}_8$). The STF method offers a large improvement, since it exploits also the STF part of the preamble. Finally, the proposed SMS method with $L_{\text{s}} = 128$, non-genie-aided, and initialized with SXC, is the best performer: the estimated channel correlation together with the knowledge of the noise variance helps in decreasing the estimation error.

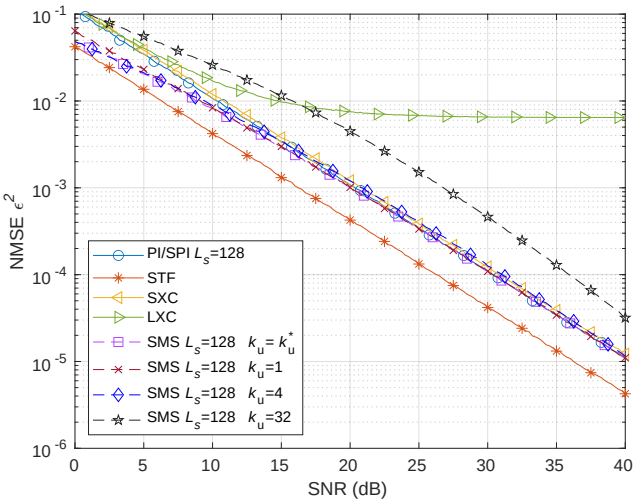

Fig. 6. NMSE of estimation methods for the channel [16].

Note that, in Fig. 4, the SMS method uses the optimal k_{u}^* value that minimizes the NMSE for a certain SNR (found by exhaustive search in the range $-3 \le \log_{10} k_{\text{u}} \le 2.5$). For completeness, results are reported also when k_{u} is fixed at either 1, 4, or 32: in this specific channel, $k_{\text{u}} = 32$ is a good choice at high SNR, while $k_{\text{u}} = 4$ is good choice at low SNR.

Figure 5 compares the NMSE of SPI and SMS methods as a function of the channel sparsity assumed by the estimator, for the same simulated channel (61), which has $S_{\text{C}} = 20$ nonnull taps. We note that both the SPI and SMS methods are sensitive to underestimation of the channel sparsity: indeed, when the estimators assume $L_{\text{s}} = 19$ nonnull channel taps, the NMSE performance has an error floor. On the other hand, the proposed SMS method is less sensitive than the SPI method to the overestimation of the channel sparsity: when the estimators assume $L_{\text{s}} = 2S_{\text{C}} = 40$ nonnull channel taps, the performance gap from the optimal genie-aided case ($L_{\text{s}} = S_{\text{C}} = 20$) is negligible for the proposed SMS method, while the gap is about 5 dB for the SPI method. In addition, when $L_{\text{s}} > 40$, the performance gap of the SPI method increases, while the gap of the proposed SMS method remains negligible. Hence, the proposed SMS method can safely use an overestimation of the channel sparsity, without losing in terms of NMSE performance.

The NMSE performance for the channel in [16] is shown in Fig. 6: the performance comparison is similar to that of Fig. 4, with two minor differences. First, the best performance is obtained by the STF method, whose complexity and latency are larger than the proposed SMS method, because the STF method uses $N_{\text{S}} + N_{\text{b}} = 26$ received blocks, while the proposed SMS method uses $N_{\text{b}} = 9$ blocks only. Second, the optimal value k_{u}^* varies differently for the two channel types: Figure 7 shows that, for the channel (61), the optimal value k_{u}^* increases with the SNR from $k_{\text{u}} \approx 4$ to $k_{\text{u}} \approx 40$, while for the channel in [16] the optimal value reduces with the SNR, from $k_{\text{u}} \approx 4$ to nearly zero. For both channels, in Fig. 7 we also plot the least-squares (LS) fitting curve, which could be used when the channel estimator knows the channel model.

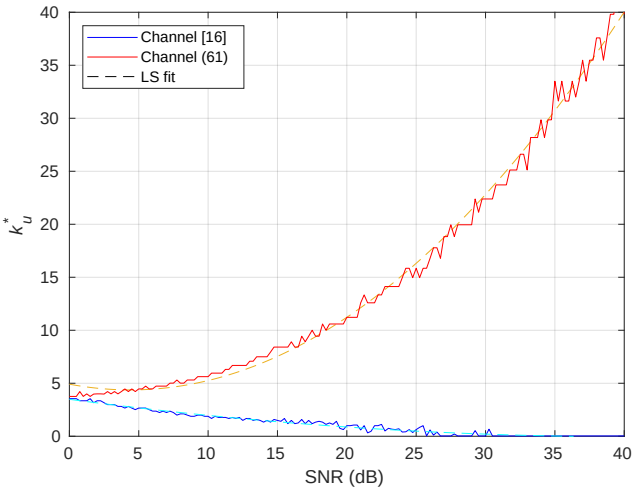

Fig. 7. Optimal value k_u^* as a function of SNR for both channels with SMS estimation.

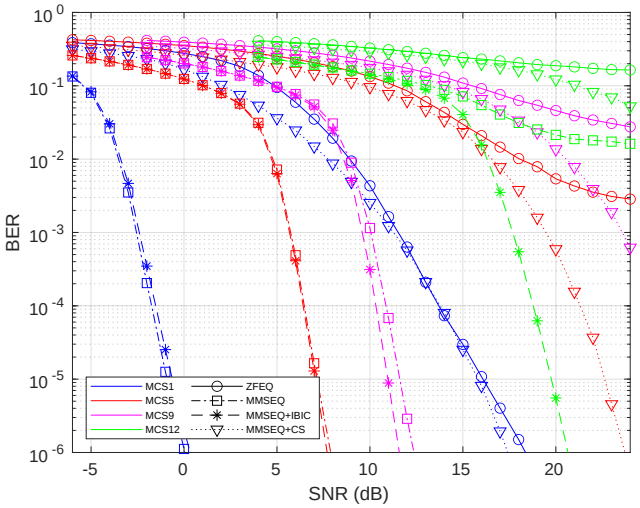

Fig. 8. BER on channel (61) with perfect CIR knowledge.

In addition, by observing the SMS results in Figs. 4–6, we can conclude that the value $k_u = 4$ is well fit to obtain a valid SMS estimate for both channels and for both low and high SNR: indeed, although Figure 4 shows some NMSE performance loss at high SNR for the channel (61), the NMSE value is so low that there is no significant difference between the true channel and the estimated channel.

5.2 Detection Performance

Detection performance has been evaluated in terms of bit error rate (BER) on multipath channels: we have used the channel model (61), which generates a large IBI, since its length significantly exceeds that of the GI. In Figs. 8–14 we present the results of such simulations. We simulated ZF and MMSE equalizers for some selected MCSs (MCS1: BPSK with repetition; MCS5: BPSK; MCS9: QPSK; MCS12: 16QAM). For MMSE equalization, we have also considered the cases with and without IBI cancellation or CIR shortening. We have chosen the MCS set so as to simulate all modulation types and the lowest and highest coding rates. In the legends of Figs. 8–14, ZF equalizer is indicated as "ZFEQ", MMSE equalizer is indicated as "MMSEQ", IBI cancellation as "IBIC", and CIR shortening as "CS".

Figure 8 shows the performance achieved with perfect CIR knowledge. MMSE equalization significantly improves the performance for all modes with respect to ZF equalization. For a BER of 10^{-5}, the gain is 17 dB for MCS1, while for the other tested modes the BER of ZF presents an error floor. For MCS12, also the MMSE equalizer without other corrections experiences an error floor, which is lower than for ZF. The addition of IBI cancellation to MMSE equalization yields a variable gain. While for MCS1 there is a slight loss of 0.25 dB, for MCS5 there is a slight advantage of 0.1 dB, which becomes appreciable for MCS9 (0.65 dB); for MCS12, MMSE equalizer with IBI cancellation does not present any error floor. The results also show that, for this particular channel, CIR shortening has limited performance.

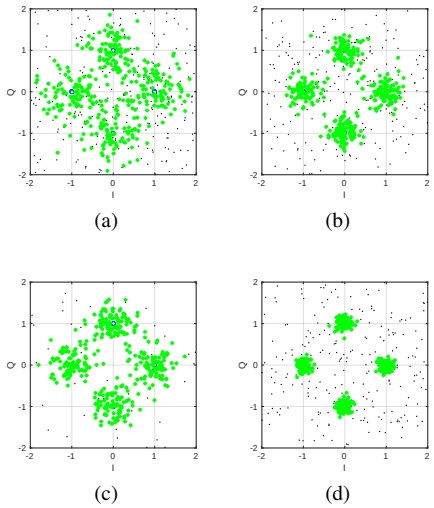

Fig. 9. Scatter plots for MCS9 in channel (61): received (black) and equalized (green) signals. (a) ZF equalizer only; (b) MMSE equalizer only; (c) CIR shortening plus MMSE equalizer; (d) IBI cancellation plus MMSE equalizer.

Indeed, for MCS1, MCS5, and MCS9, the performance of MMSE equalization with CIR shortening is closer to that of ZF equalization than to that of MMSE with IBI cancellation.

We attribute the bad performance of CIR shortening mostly to the shortening filter, which compresses most of the CIR energy within the GI interval, but at the same time generates large peaks in the frequency response. These peaks amplify the effects of noise, similarly to the noise amplification of the ZF equalizer. For example, in Fig. 9, we show the received QPSK constellation for MCS9, before and after equalization, at an SNR of 24 dB, using perfect CIR knowledge of channel (61). For the ZF equalizer (Fig. 9(a)), the four clouds are barely distinguishable, while for the MMSE equalizers (Figs. 9(b)–9(d)) the four clouds are evident. The MMSE with IBI cancellation (Fig. 9(d)) gives a lower spread of the clouds, with respect to MMSE without IBI cancellation (Fig. 9(b)) and to MMSE with CIR shortening (Fig. 9(c)).

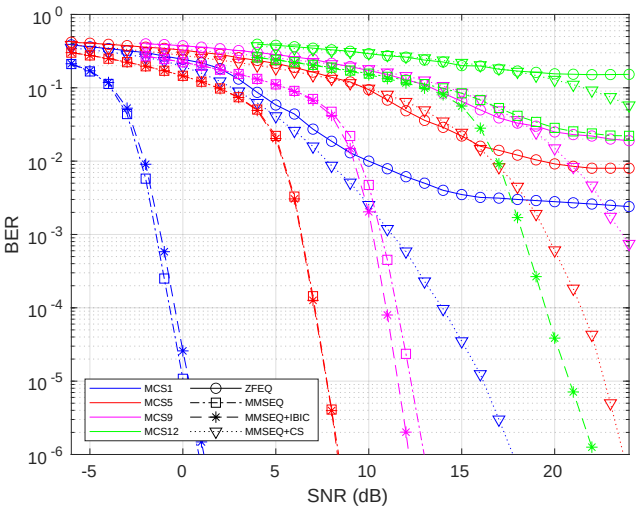

Fig. 10. BER on channel (61) with SXC estimation.

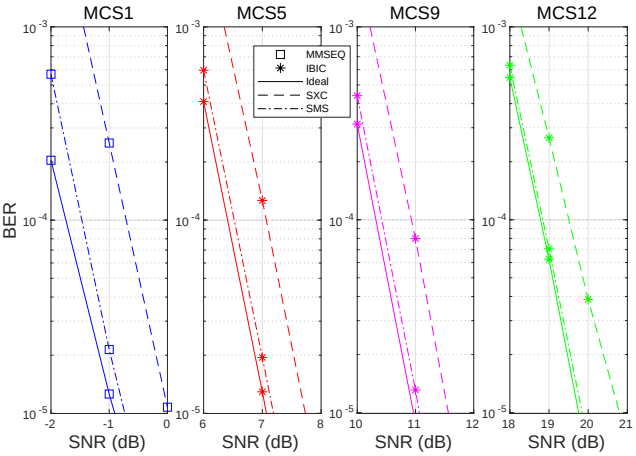

Fig. 12. BER on channel (61) with different CIR estimators.

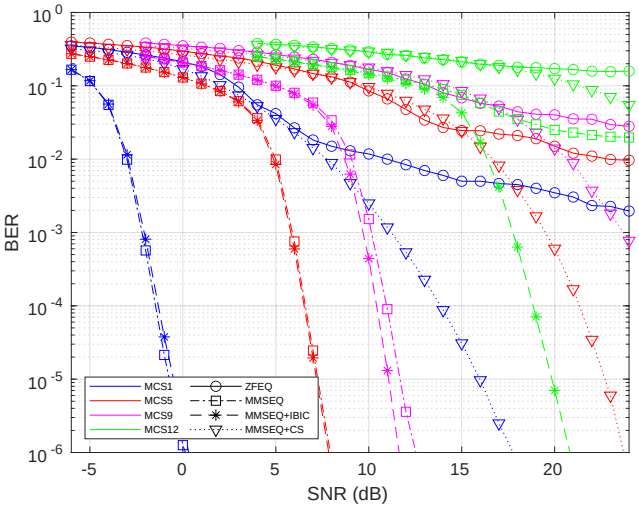

Fig. 11. BER on channel (61) with SMS estimation.

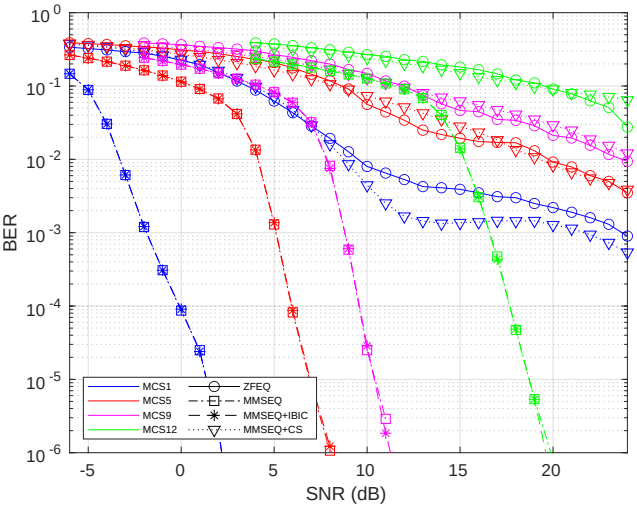

Fig. 13. BER on channel [16] with SMS estimation.

Figures 10 and 11 present the results for conventional SXC and the proposed SMS methods, respectively. The curves have the same trend of Fig. 8 (perfect CIR knowledge), except for the BER of MCS1 with ZF equalization, which now presents an error floor for both channel estimation methods. This error floor is caused by the ZF amplification of the channel estimation error.

The performance of the different CIR estimation methods is compared in Fig. 12, for MCS1 with MMSE equalizer without IBI cancellation, and for MCS5, MCS9, MCS12 with MMSE equalizer with IBI cancellation. In all cases, the proposed SMS estimator outperforms the conventional SXC estimator, and achieves the performance of the perfect CIR knowledge. SXC suffers an SNR loss of 0.60–1.05 dB from the perfect knowledge, while our SMS method suffers of a reduced loss (0.10–0.20 dB) from the perfect knowledge. Therefore, the proposed SMS channel estimator enables improved performance in the simulated scenarios, with an SNR gain of 0.50–0.95 dB with respect to conventional SXC.

For comparison, we plot in Fig. 13 the results obtained for SMS estimation when channel [16] is used. For this case, there is a reduced amount of IBI to be canceled: therefore, IBI cancellation does not improve the BER performance. Moreover, even for this channel, both ZF equalization and CIR shortening suffer from noise enhancement issues, resulting in a large BER.

5.3 Performance of LLR Update

Figure 14 compares the receiver performance when using the proposed LLR update (53) or the conventional LLR (60). In both cases, perfect CIR knowledge is assumed. The performance gain when using (53) in place of (60) amounts to 1.5 dB for MCS1, 0.5 dB for MCS5, 0.4 dB for MCS9, and 0.4 dB for MCS12. This performance gain of the proposed LLR update is caused by the correct inclusion of the interference power together with the noise power, differently from the conventional LLR.

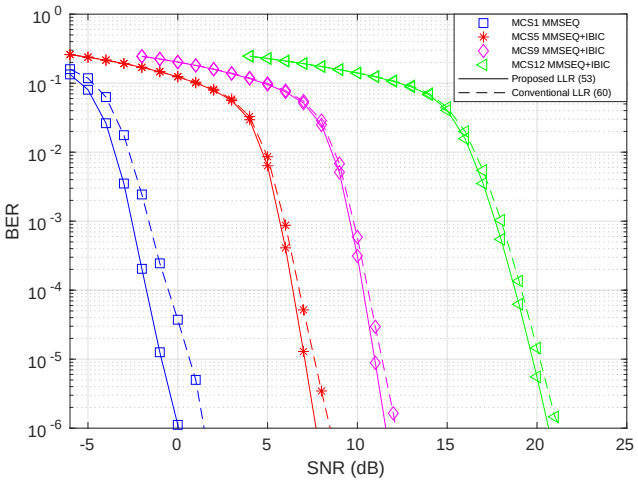

Fig. 14. Effect of LLR expression on the BER on channel (61).

6. Conclusion

In this paper we have presented some methods to improve the performance of IEEE 802.11ad receivers operating in SC mode, when the CIR is exceedingly long. The first method concerns channel estimation: we use the channel sparsity to propose an improved MMSE-based channel estimator. A second method allows to mitigate the effect of a long CIR by employing MMSE equalization with interference cancellation and circularity restoration. Our results show that IBI cancellation is useful for QPSK modes and necessary for 16QAM modes. We have also proposed an LLR expression that includes the presence of residual interference. Simulation results with multipath channels show that the proposed CIR estimator and the proposed equalizers outperform the conventional methods. Future work may include the extension of the proposed methods to similar standards, such as IEEE 802.11ay [17], [39].

Acknowledgments

This work was supported by MIUR under the PRIN 2017 “Liquid Edge” project and by the University of Perugia “Fondi ricerca di base 2020” project (UA.PG.DING RICBA20GBAR) and “Fondi ricerca di base 2022” project EFESO.

References

[1] NITSCHE, T., CORDEIRO, C., FLORES, A. B., et al. IEEE 802.11ad: Directional 60 GHz communication for multi-gigabit-per-second Wi-Fi. *IEEE Communications Magazine*, 2014, vol. 52, no. 12, p. 132–141. DOI: 10.1109/MCOM.2014.6979964

[2] CORDEIRO, C., AKHMETOV, D., PARK, M. IEEE 802.11ad: Introduction and performance evaluation of the first multi-gbps WiFi technology. In *Proceedings of the 2010 ACM International Workshop on mmWave Communications (mmCom)*. Chicago (USA), 2010, p. 3–8. DOI: 10.1145/1859964.1859968

[3] IEEE COMPUTER SOCIETY. *Amendment 3: Enhancements for Very High Throughput in the 60 GHz Band (Standard)*. IEEE Std. 802.11ad. 628 pages. 2012. DOI: 10.1109/IEEESTD.2012.6392842

[4] AGGARWAL, S., GHOSHAL, M., BANERJEE, P., et al. An experimental study of the performance of IEEE 802.11ad in smartphones. *Computer Communications*, 2021, vol. 169, p. 220–231. DOI: 10.1016/j.comcom.2021.01.006

[5] METROLINQ. *60GHz Wireless PTP/PTMP – IgniteNet*. [Online] Cited 2023-06-13. Available at: https://www.ignitenet.com/technology/metrolinq/

[6] MIKROTIK. *Routers and Wireless – 60 GHz Products*. [Online] Cited 2023-06-13. Available at: https://mikrotik.com/products/group/60-ghz-products

[7] QUALCOMM. *QCA6335 – 802.11ad MAC Baseband Transceiver*. [Online] Cited 2023-06-13. Available at: https://www.qualcomm.com/products/technology/wi-fi/qca6335

[8] GAO, B., ZHANG, C., Z., JIN, D., et al. Compressed SNR-and-channel estimation for beam tracking in 60-GHz WLAN. *China Communications*, 2015, vol. 12, no. 6, p. 46–58. DOI: 10.1109/CC.2015.7122480

[9] SHAHAM, S., DING, M., KOKSHOORN, M., et al. Fast channel estimation and beam tracking for millimeter wave vehicular communications. *IEEE Access*, 2019, vol. 7, p. 141104–141118. DOI: 10.1109/ACCESS.2019.2944308

[10] YE, B., ZHANG, Z. Improved pilot design and channel estimation for 60GHz OFDM based on IEEE 802.11.ad. In *Proceedings of 2013 IEEE Wireless Communications Networks Conference (WCNC)*. Shanghai (China), 2013, p. 4129–4133. DOI: 10.1109/WCNC.2013.6555239

[11] LIU, C.-Y., SIE, M.-S., LEONG, E. W. J., et al. Dual-mode all-digital baseband receiver with a feed-forward and shared-memory architecture for dual-standard over 60 GHz NLOS channel. *IEEE Transactions on Circuits and Systems I*, 2017, vol. 64, no. 3, p. 608–618. DOI: 10.1109/TCSI.2016.2615084

[12] WU, C.-F., LIU W.-C., TSUI, C.-C., et al. Golay-correlator window-based noise cancellation equalization technique for 60-GHz wireless OFDM/SC receiver. *IEEE Transactions on Very Large Scale Integration (VLSI) Systems*, 2016, vol. 24, no. 11, p. 3323–3333. DOI: 10.1109/TVLSI.2016.2544884

[13] LIU, W.-C., WEI, T.-C., HUANG, Y.-S., et al. All-digital synchronization for SC/OFDM mode of IEEE 802.15.3c and IEEE 802.11ad. *IEEE Transactions on Circuits and Systems I*, 2015, vol. 62, no. 2, p. 545–553. DOI: 10.1109/TCSI.2014.2361035

[14] GUAN, X., ZHANG, C., JIN, D. High-speed structure of channel estimation and equalization for 60 GHz SC-FDE transmission. In *Proceedings of International Conference on Computational Problem-Solving (ICCP)*. Jiuzhai (China), 2013, p. 211–214. DOI: 10.1109/ICCPS.2013.6893577

[15] BLUMENSTEIN, J., MILOS, J., POLAK, L., et al. IEEE 802.11ad SC-PHY layer simulator: Performance in real-world 60 GHz indoor channels. In *Proceedings of 2019 IEEE Nordic Circuits and Systems Conference (NORCAS)*. Helsinki (Finland), 2019, p. 1–4. DOI: 10.1109/NORCHIP.2019.8906960

[16] LIU, P., BLUMENSTEIN, J., PEROVIĆ, N. S., et al. Performance of generalized spatial modulation MIMO over measured 60GHz indoor channels. *IEEE Transactions on Communications*, 2018, vol. 66, no. 1, p. 133–148. DOI: 10.1109/TCOMM.2017.2754280

[17] POLAK, L., MILOS, J., ZEDKA, R., et al. BER and throughput performances of IEEE 802.11ay SC-PHY over measured 60 GHz indoor channels. *Telecommunication Systems*, 2022, vol. 80, p. 573–587. DOI: 10.1007/s11235-022-00928-9

[18] RENDEVSKI, N., CASSIOLI, D. BER of IEEE 802.11ad OFDM radios vs. carrier frequency in real 60 GHz indoor channels. In *Proceedings of 2014 IEEE International Conference on Communications (ICC)*. Sydney (Australia), 2014, p. 5878–5883. DOI: 10.1109/ICC.2014.6884260

[19] HWANG, T., LI, Y. Iterative cyclic prefix reconstruction for coded single-carrier systems with frequency-domain equalization (SC-FDE). In *Proceedings of 57th IEEE Semiannual Vehicular Technology Conference (VTC Spring)*. Jeju (Korea), 2003, vol. 3, p. 1841–1845. DOI: 10.1109/VETECS.2003.1207142

[20] HAYASHI, K., SAKAI, H. Interference cancellation schemes for single-carrier block transmission with insufficient cyclic prefix. *EURASIP Journal on Wireless Communications and Networking*, 2007, vol. 2008, p. 1–12. DOI: 10.1155/2008/130747

[21] KUMARI, P., GONZALEZ-PRELCIC, N., HEATH, R. W. Investigating the IEEE 802.11ad standard for millimeter wave automotive radar. In *Proceedings of IEEE 82nd Vehicular Technology Conference (VTC Fall)*. Boston (USA), 2015, p. 1–5. DOI: 10.1109/VTCFall.2015.7390996

[22] GROSSI, E., LOPS, M., VENTURINO, L. An iterative interference cancellation algorithm for opportunistic sensing in IEEE 802.11ad networks. In *Proceedings of IEEE 8th International Workshop on Computational Advances in Multi-Sensor Adaptive Processing (CAMSAP)*. Guadeloupe (France), 2019, p. 141–145. DOI: 10.1109/CAMSAP45676.2019.9022460

[23] LI, W., JAGANNATH, R., GUAN, Y. L., et al. A novel design of multi-user sequence set for joint vehicular radar-communication based on Oppermann family. *Digital Signal Processing*, 2023, vol. 141, p. 1–11. DOI: 10.1016/j.dsp.2023.104119

[24] CHENG, S., PAHLAVAN, K., WEI, H., et al. A study of interference analysis between mmWave radars and IEEE 802.11ad at 60 GHz bands. *International Journal of Wireless Information Networks*, 2022, vol. 29, no. 3, p. 222–231. DOI: 10.1007/s10776-022-00564-9

[25] SÜMEN, G., GÖRÇIN, A., QARAQE, K. A. Measurement-based modulation classification in unlicensed millimeter-wave bands. In *Proceedings of 2023 IEEE Wireless Communications and Networking Conference (WCNC)*. Glasgow (UK), 2023, p. 1–6. DOI: 10.1109/WCNC55385.2023.10119008

[26] ZHAO, S., LIU, W., LEI, J., et al. An approach of measuring velocity based on auto-correlation in a single frame for IEEE 802.11ad. *Electronics Letters*, 2022, vol. 58, no. 25, p. 1019–1021. DOI: 10.1049/ell2.12670

[27] ABD, R. I., KIM, K. S. Protocol solutions for IEEE 802.11bd by enhancing IEEE 802.11ad to address common technical challenges associated with mmWave-based V2X. *IEEE Access*, 2022, vol. 10, p. 100646–100664. DOI: 10.1109/ACCESS.2022.3208235

[28] CHATTOPADHYAY, A., CHANDRA, A. IEEE 802.11ac vs 802.11ad for V2X: How many frames can we aggregate? In *Proceedings of 2022 IEEE 33rd Annual International Symposium on Personal, Indoor and Mobile Radio Communications (PIMRC)*. Kyoto (Japan), 2022, p. 913–918. DOI: 10.1109/PIMRC54779.2022.9977545

[29] MARTIN, R. K., DING, M., EVANS, B. L., et al. Efficient channel shortening equalizer design. *EURASIP Journal on Applied Signal Processing*, 2003, vol. 2003, no. 13, p. 1–12. DOI: 10.1155/S1110865703307024

[30] DARSENA, D., VERDE, F. Minimum-mean-output-energy blind adaptive channel shortening for multicarrier SIMO transceivers. *IEEE Transactions on Signal Processing*, 2007, vol. 55, no. 12, p. 5755–5771. DOI: 10.1109/TSP.2007.900087

[31] BENOTMANE, N. B., ELAHMAR, S. A., DAYOUB, I., et al. Improved eigenfilter design method for channel shortening equalizer in TH-UWB. *IEEE Transactions on Vehicular Technology*, 2018, vol. 67, no. 8, p. 7749–7753. DOI: 10.1109/TVT.2018.2822178

[32] DJEBBARI, A., ELAHMAR, S. A. Improved CSE with DLS-MMSE criteria in TH-UWB system. *Journal of Telecommunications and Information Technology*, 2022, vol. 1, p. 93–98. DOI: 10.26636/jtit.2022.151421

[33] ZHANG, C., XIAO, Z., WU, H. et al. Performance analysis on the OFDM PHY of IEEE 802.11ad standard. In *Proceedings of 2011 International Conference on Computational Problem-Solving (ICCP)*. Chengdu (China), 2011, p. 708–713. DOI: 10.1109/ICCPS.2011.6089947

[34] KIMURA, R., FUNADA, R., NISHIGUCHI, Y., et al. Golay sequence aided channel estimation for millimeter-wave WPAN systems. In *Proceedings of 2008 IEEE 19th International Symposium on Personal, Indoor and Mobile Radio Communications (PIMRC)*. Cannes (France), 2008, p. 1–5. DOI: 10.1109/PIMRC.2008.4699819

[35] DE CARVALHO, E., SLOCK, D. Cramer-Rao bounds for semi-blind, blind and training sequence based channel estimation. In *Proceedings of 1997 1st IEEE Workshop on Signal Processing Advances in Wireless Communications (SPAWC)*. Paris (France), 1997, p. 129–132. DOI: 10.1109/SPAWC.1997.630172

[36] COON, J., BEACH, M., MCGEEHAN, J. Optimal training sequences for channel estimation in cyclic-prefix-based single-carrier systems with transmit diversity. *IEEE Signal Processing Letters*, 2004, vol. 11, no. 9, p. 729–732. DOI: 10.1109/LSP.2004.833485

[37] ALKHATEEB, A., EL AYACH, O., LEUS, G., et al. Channel estimation and hybrid precoding for millimeter wave cellular systems. *IEEE Journal on Selected Topics in Signal Processing*, 2014, vol. 8, no. 5, p. 831–846. DOI: 10.1109/JSTSP.2014.2334278

[38] HENDERSON, H. V., SEARLE, S. R. On deriving the inverse of a sum of matrices. *SIAM Review*, 1981, vol. 23, no. 1, p. 53–60. DOI: 10.1137/1023004

[39] ZHOU, P., CHENG, K., HAN, X., et al. IEEE 802.11ay-based mmWave WLANs: Design challenges and solutions. *IEEE Communications Surveys and Tutorials*, 2018, vol. 20, no. 3, p. 1654–1681. DOI: 10.1109/COMST.2018.2816920

About the Authors ...

Giuseppe BARUFFA was born in Perugia, Italy, in 1970. He received the Laurea degree in Electronic Engineering and the Ph.D. degree in Telecommunications from the University of Perugia, Perugia, Italy, in 1996 and 2001, respectively. In 2005, he visited the Swiss Federal Polytechnic of Lausanne, Lausanne, Switzerland. Since 2005, he has been an Assistant Professor with the Department of Engineering, University of Perugia. His main research interests include digital television broadcasting, joint source/channel video coding, and LPWAN sensor networks.

Luca RUGINI was born in Perugia, Italy, in 1975. He received the Laurea degree (cum laude) in Electronic Engineering and the Ph.D. degree in Telecommunications from the University of Perugia, Perugia, Italy, in 2000 and 2003, respectively. In 2007, he visited Delft University of Technology, Delft, The Netherlands. He is currently an Assistant Professor with the Department of Engineering, University of Perugia. His research interests lie in the area of signal processing for communications. Dr. Rugini serves as an Area Editor for Digital Signal Processing from 2023. He served as an Associate Editor for the IEEE Signal Processing Letters from 2014 to 2018, for Digital Signal Processing from 2012 to 2022, and for the EURASIP Journal on Advances in Signal Processing from 2015 to 2022.